June 2020

Fog forecasting in HARMONIE

a case study to current issues with the overestimation of fog in HARMONIE

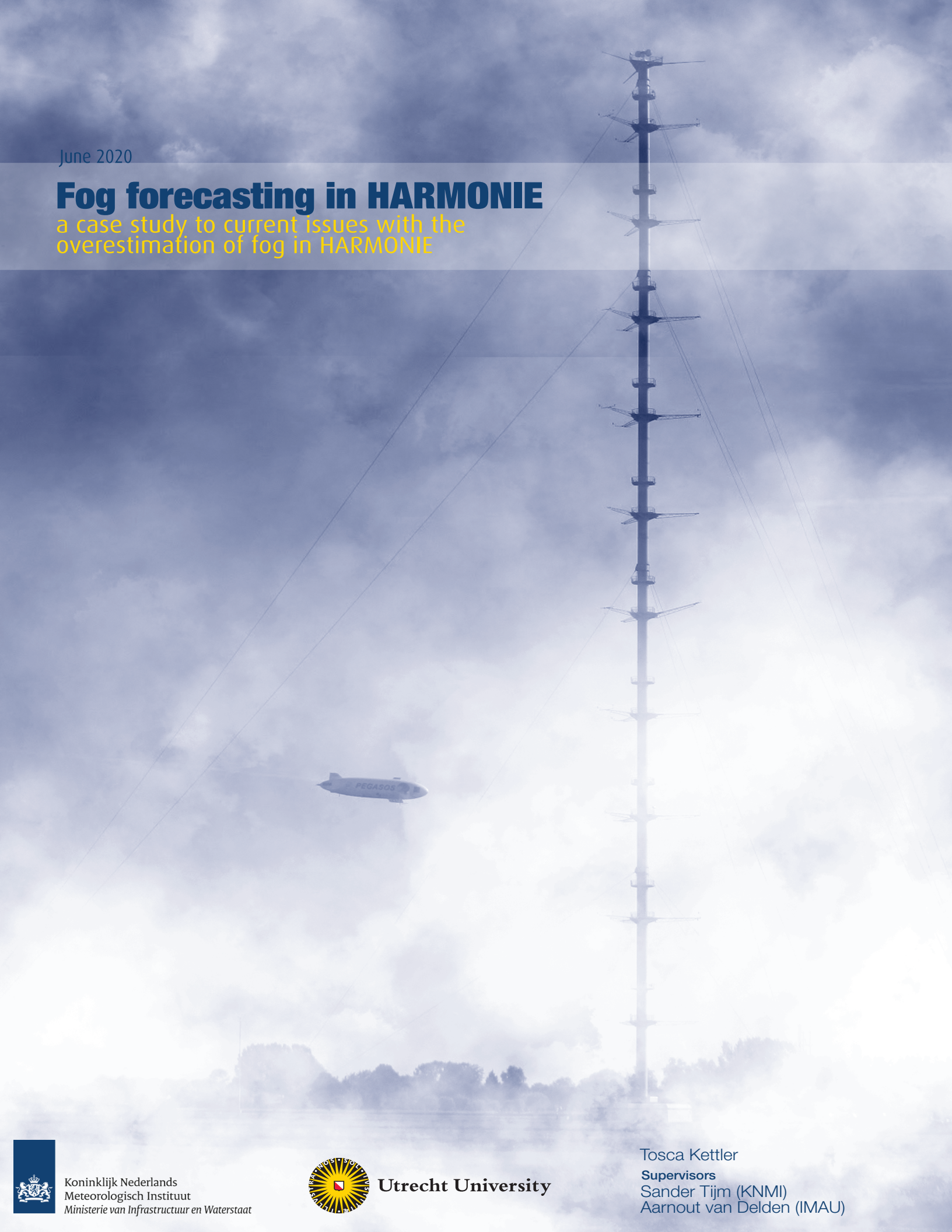

Koninklijk Nederlands
Meteorologisch Instituut
Ministerie van Infrastructuur en Waterstaat

Utrecht University

Tosca Kettler

Supervisors
Sander Tijm (KNMI)
Aarnout van Delden (IMAU)

Contents

1 Abstract

A recurring issue in HARMONIE-AROME is the overestimation of the occurrence of dense fog over the Netherlands. In this thesis, the performance of Harmonie on simulating radiation fog is studied by comparison of simulated fog to observed fog at the Cabauw observatory. By evaluating the representation of physical processes related to radiation fog formation in HARMONIE-AROME, acute issues are addressed that may lead to erroneous forecasting. The main focus lies on the representation of fog in the longwave radiation scheme and its dependence on the amount of cloud condensation nuclei. After analysis of a fog case study in which the fog simulated by HARMONIE-AROME is compared to Cabauw observations, the 1D model MUSC is used to evaluate the fog evolution in more detail for testing the performance of new parametrizations. From these experiments appears that the overestimation of fog is correlated to too strong longwave cooling by the fog. Based on the outcomes of many MUSC experiments, the HARMONIE-AROME case study is rerun in experiments with adaptations based on cloud longwave emissivity (0.096 instead of 0.144), longwave cloud inhomogeneity (0.7 instead of 1) and the number of cloud condensation nuclei (10-50 cm^{-3} instead of 300 cm^{-3} over land and 100 cm^{-3} over sea). The results of this study show that a reduction of the longwave emissivity combined with reduced CCN leads to a large improvement in the behavior of simulated fog.

2 Acknowledgements

I wish to show my enormous gratitude to my daily supervisor at the KNMI, Sander Tijm, as his enthusiastic assistance and worthy experience were invaluable during this research. When I ran into a trouble spot or had questions about my research or writing, he was always willing to give his time. This thesis could not have existed without his constructive feedback and passionate input, and his numerous insights have made my research at the KNMI an inspiring experience.

I also wish to thank my first supervisor at Utrecht University, Aarnout van Delden. Moreover, I would like to acknowledge Michiel van den Broeke as the second reader of this thesis. I am greatful that they are willing to give their time to provide me with feedback on my thesis. Furthermore, the knowledge and skills I obtained following the lectures provided by them, and by many other staff members of the IMAU during my master Climate Physics at Utrecht University were extremely useful during this research.

Moreover, I wish to thank the KNMI for giving me the opportunity to do this project, as well as various people at the KNMI for their contribution to this project. I am very thankful to Bram van 't Veen, who helped me to master working with the Linux environment and with Grib files in the initial phase of my research, and Bert van Ulft, who helped me with many complications I encountered setting up the Musc environment for the experiments. Furthermore, I would like to thank the many meteorologists and researchers in the weather room who helped me with many issues and made me feel at home.

3 Introduction

The Royal Netherlands Meteorological Institute (KNMI) is the Dutch national weather service, and the national research information centre for meteorology, climate, air quality, and seismology. The primary tasks of KNMI are weather forecasting and monitoring of air quality, climate changes and seismic activity. KNMI advises on and warns society for topics related to these fields, thereby contributing to the safety, accessibility, sustainability and prosperity of the Netherlands. Since 2012, HARMONIE-AROME (HIRLAM ALADIN Research on Meso-scale Operational NWP in Europe, hereafter referred to as Harmonie) is the main operational weather forecast system at KNMI. KNMI runs Harmonie version 40h1.1.1 every three hours, centered at Cabauw with a 2.5 km horizontal resolution and a 65-level vertical resolution. Although Harmonie has proven its value, there are still important deficiencies.

Fog and visibility are among the most difficult and important parameters that are simulated with Harmonie. The demand for detailed forecasts on short timescales is high, as (dense) fog can be hazardous to many core parts of the Dutch society including aviation, shipping and nearly all forms of surface transport. Furthermore, the sensitivity of many other meteorological conditions to the presence of fog is large. Fog processes, on their turn, are highly complex and sensitive to many thermodynamic and dynamical factors that vary on local basis. The formation and evolution of fog depends on precise balances between these processes, causing fog to be extremely variable in time and space.

Despite its large economical and societal impact, the skill in forecasting the formation and development of fog is still relatively low (Steeneveld, Ronda, and Holtslag 2015). A recurring issue in Harmonie is the overestimation of the occurrence of dense fog over the Netherlands (de Rooy 2014, Marthinsen 2015, Tijm 2018). Harmonie repeatedly produced large and persistent fog layers over sea, which were not observed. The underlying causes are hard to discover as so many meteorological mechanisms are involved. Shortcomings may be a consequence of uncertainties in the related physics, as relevant measurements on natural fogs are scarce and often specific for a micro-meteorological domain. Current parametrizations are sometimes based on different domains or have not been adjusted to climatological

changes in the Netherlands over the past decades. On top of that, the large gap between horizontal and vertical resolutions of Harmonie and the characteristic length and height scales of fog requires the description of local processes in a large domain, which is highly challenging.

In this thesis, the performance of Harmonie on simulating radiation fog is studied by comparison of simulated fog to observed fog at the Cabauw observatory. By evaluating the representation of physical processes related to radiation fog formation in Harmonie, acute issues are addressed that may lead to erroneous forecasting. Of all the issues raised in this thesis, the main focusses are on the representation of fog in the longwave radiation scheme in Harmonie and its dependence on the amount of cloud condensation nuclei. This thesis aims to contribute to a basis for further improvement of Harmonie, by addressing discrepancies and proposing adjustments to the currently used parametrizations that aim to improve the physical correctness of fog simulations.

To realize this objective, the rest of this thesis is structured as follows: Chapter 4 introduces the reader to fog, covering general concepts related to fog as well as the underlying physics. Chapter 5 provides a description of Harmonie, emphasizing on model aspects relevant to fog forecasting. Chapter 6 describes the observational data provided by the Cabauw observatory, that has been used in this study. In Chapter 7, a general outline of the methods used is given, covering the set-up of different experiments and introducing MUSC, the 1-dimensional version of Harmonie. Chapter 8 shows the results of a case study during a foggy night, in which the differences between Harmonie forecasts and Cabauw observations related to fog are explored. In Chapter 9, the results of MUSC experiments are shown to address the impact of different parametrizations. Chapter 10 shows Harmonie runs using adjusted parametrizations, to test whether their application leads to improved performance. Chapter 11 gives an overview of discussion points, and Chapter 12 summarizes the conclusions and recommendations following from this research.

4 Introduction to fog

4.1 Basic principles

Fog may be defined as a visible aggregate of minuscule water droplets or ice crystals, reducing horizontal visibility to less than one kilometer. It can be categorized as a type of (stratus) cloud, discriminated from other clouds by the fact that fog is based at the Earth's surface. Fog is distinguished from drizzle as it does not fall to the ground. Fog intensity is expressed in terms of visibility, which describes the opacity of the atmosphere by any light-absorbing constituent. The measurement of visibility does therefore not isolate the presence of fog, as it is subject to environmental factors. In addition to water and ice droplets, visibility can be reduced by the presence of aerosols such as smoke, volcanic ash, dust and sand (OFCM 2005). The standard measure of visibility is the meteorological optical range (MOR), which is defined in section 4.2.2.

Fog is formed when the air temperature becomes roughly equal to the dewpoint temperature. This may happen when the ambient air temperature drops, when the dewpoint temperature rises due to addition of moisture to the air, or due to the vertical mixing of air parcels with different temperatures and humidities (Duynkerke 1991). Water vapor then condenses into minute water droplets on condensation nuclei such as salt, dust and ice. The visibility reduction induced by fog increases with increasing droplet number and water mass in a given volume of air (Gultepe, Isaac, and Strawbridge 2001), characteristics that are described by a fog's droplet size distribution (DSD). The DSD in fog depends on its formation mechanism and on the concentration of cloud condensation nuclei (CCNs) (American Meteorological Society 2012). The CCNs are used as the cores of water droplets, allowing water to attach to the CCN. When an air mass contains a higher concentration of CCNs, an increased amount of cloud droplets will form. The presence of many CCNs leads to the formation of a large number of small droplets that settle relatively slowly, and consequently to lower visibility. Therefore, a lower amount of CCN also decreases the efficiency of the precipitation and thereby extends the lifetime of fog. In contrast,

low CCN concentrations can limit fog growth, as a lower amount of larger water droplets are formed (Gultepe, Isaac, and Strawbridge 2001).

Fog processes are highly complex and sensitive to many thermodynamic and dynamical factors that vary on local basis. The formation and evolution of fog depends on precise balances between these processes, causing fog to be extremely variable in time and space. The most important factors governing fog formation are the following (Duynkerke 1991):

- Cooling of moist air by radiative flux divergence
- Vertical mixing of moisture and heat (including dew deposition)
- Horizontal and vertical wind
- Advection
- Vegetation
- Moisture and heat transport in soil
- Surface configuration

The further development of the fog may be influenced by the following factors (Duynkerke, 1991):

- Longwave radiative cooling at the fog top
- Droplet configuration
- Fog microphysics
- Shortwave radiation

Over the past three decades, the number of foggy days per year declined from 80 to 40 days per year in the Netherlands. Dense fog events with visibilities under 200m also declined by 50%, from 30 to 15 days per year (Vautard, Yiou, and Oldenborgh 2009). This decrease is correlated to reduced aerosol (mainly sulphur dioxide) emissions, a drying summer trend and circulation changes (Van Oldenborgh, Yiou, and Vautard 2010, Van Beelen and van Delden 2012). Most fog is observed from October until February, when long winter nights promote fog formation (Duynkerke 1991). Fog generally forms in a

cool, stable air mass that is trapped underneath warm air. The categorization of different types of fog is based on the fog's primary formation mechanism and environmental conditions. The most common types in the Netherlands are radiation fog, advection fog and frontal fog (Duynkerke 1991).

Radiation fog typically forms under clear skies at night, in moist air with relatively low wind speeds. Due to a net infrared radiative heat loss, earth's surface cools rapidly after sunset. This surface heat loss is largely balanced by upward conduction of heat through the upper few centimeters of the soil, and by turbulent transport of heat and moisture towards the surface. The conduction of heat from the adjacent air to the surface causes the air temperature to fall. The cooling of air near the ground promotes thermal stability, thereby weakening and sometimes stopping low-level turbulence. When the air temperature reaches the dew point temperature, a fog layer may form. Often, the fog layer initially forms at the surface and thickens over time as long as the radiative cooling continues. When the optical depth of the fog increases, the maximum in radiative cooling becomes displaced from the surface to the top of the fog (Duynkerke 1991).

During long winter nights, thick and long-lasting fog layers can develop while summer radiation fog is usually thinner. Fog generally develops under low wind speeds, as wind is required to drive a sufficient supply of sensible and latent heat towards the surface, but too high wind speeds can lead to mixing of the fog layer with dryer air and thereby to dissolution of the fog. Furthermore, high soil wetness substantially promotes the formation of a fog layer (Duynkerke 1991, 1999). Radiation fog usually consists of small droplets with a droplet size distribution (DSD) between one and ten μm (Duthon, Colomb, and Bernardin 2019). During field campaigns dedicated to fog life cycle observation near Paris, Mazoyer et al. (2019) found that typical droplet number concentrations in radiation fog are 73-131 cm^{-3} for thin fog layers (maximum fog height $<$ 18m), and 49-98 cm^{-3} for thick fog layers. Observed liquid water content varied between 0.01 and 0.06 $\frac{g}{m^3}$

Advection fog typically forms when warm and moist air is advected over a cold surface, causing the air temperature to drop. Occasionally, it may also form due to the addition of moisture to the air when cold and moist air flows over a warm moist surface. Advection fog mostly forms over water surfaces, and can be advected to cold continental surfaces. During winter, advection fog furthermore frequently forms in

the warm sector of low pressure areas over the continents. This type of fog can last all day. Turbulent mixing is of primary importance in advection fog. Favorable conditions for the development of advection fog are surface wind speeds of 4 to 7 $\frac{m}{s}$ and a long fetch length over the cold surface. Under lower windspeeds, the turbulent mixing and therefore radiative cooling is insufficient to cause fog formation (Petersen and Nielsen 2000). Mazoyer et al. (2019) found that typical droplet number concentrations in advection fog are lower than in radiation fog (median values between 48 and 83 cm^{-3}), which is correlated to higher aerosol concentrations during radiation fog events associated to higher wind speeds.

Frontal fog typically forms when moisture is added to subfrontal cool and unsaturated air, due to evaporation of precipitation from overlying frontal clouds (Petersen and Nielsen 2000).

The processes leading to formation and dissipation of fog are extremely complex and sensitive to many local and uncertain factors. Fog forecasting is therefore challenging, and current operational short-range models often misconstrue fog events. Despite its large economical and societal impact, the skill in forecasting the formation and development of fog is still relatively low (Steeneveld, Ronda, and Holtslag 2015). HARMONIE-AROME (hereafter referred to as Harmonie) is no exception, as fog is frequently overestimated. Harmonie in particular has a tendency to over-forecast dense fog (visibility < 400 m), which was forecasted over 33 times as often as it was observed. Lighter fog (visibility between 400 and 1000 m) was forecasted 2 times as often as it was observed (Marthinsen 2015). The nature of these discrepancies is hard to discover as so many meteorological mechanisms are involved. This thesis focusses on the physical processes related to radiation fog formation and their representation in Harmonie.

4.2 Fog and radiation

The reduction of visibility due to fog is hazardous to aviation and to nearly all forms of surface transport, which a strong motivator to improve our knowledge of fog and skills in fog forecasting. The presence of a deep fog layer can substantially affect the surface budgets of shortwave and longwave radiation. This section gives an overview of the interplay between fog and radiation, and introduces some general concepts and terms that are related to fog and radiation.

4.2.1 Radiative transfer in a clear atmosphere

The radiation budget at the earth's surface consists of incoming shortwave solar radiation and longwave radiation emitted by the earth and its atmosphere. The emitted radiation spectrum by the sun and earth barely overlap, allowing an arbitrary separation between both domains around 4 μm when considering the atmosphere in terms of radiation energy transfer. A radiative flux encountering an atmospheric layer is either absorbed, scattered or transmitted. The absorptance (A_λ), reflectance (Re_λ) and transmittance (Tr_λ) are expressed in fractions of incoming radiation. Conservation of energy requires that (Cotton and van den Heever 2011):

$$A_\lambda + Re_\lambda + Tr_\lambda = 1 \tag{4.1}$$

In the clear, cloudless and fog-free atmosphere shortwave radiation is primarily absorbed by ozone and water vapor, and to a lesser extent by aerosols such as soot and carbonaceous particles. The shortest wavelengths up to 0.3 μm are almost completely absorbed by oxygen and ozone. Wavelengths in the visible region between 0.3 and 0.7 μm are largely transmitted and only weakly absorbed by ozone. Wavelengths up to 0.7 μm are furthermore attenuated by Rayleigh scattering. The wavelengths larger than 0.7 μm are mainly absorbed by water vapor in specific spectral bands, and weakly by carbon dioxide and ozone.

Longwave or infrared (IR) radiation is primarily absorbed by water vapor, carbon dioxide and ozone in different wavelength bands. Water vapor absorption bands are centered at 1.4, 1.9, 2.7, 6.3 and above 20 μm, carbon dioxide strongly absorbs wavelengths around 14.7 μm, and the ozone absorption band is centered around 9.6 μm. Wavelengths in the 'atmospheric window', a region between 8 and 14 μm are only little absorbed (Cotton and van den Heever 2011).

4.2.2 Radiative transfer in a foggy atmosphere

Clouds and fog have a large impact on visibility, earth's surface albedo and the longwave radiation budget. The radiative energy transfer in a fog is therefore of primary importance for mesoscale weather processes. The absorption and scattering of radiation diminishes the intensity of a radiative flux with distance. The Bouguer-Lambert law describes how a luminous flux of wavelength λ is attenuated by

fog:

$$\Phi = \Phi_0 * e^{-k_\lambda * d} \tag{4.2}$$

Where $k_\lambda(\lambda, DSD)$ is the wavelength dependent extinction coefficient and d is the distance between the emitting source (Φ_0) and observant receiver (Φ) of the luminous flux. The extinction coefficient is roughly constant with wavelength in the visible band, but depends on the wavelength for infrared wavelengths (Shah, Mughal, and Memon 2015).

The bulk attenuating effect of the fog can be described by the optical depth τ of the fog layer of height h, which is defined as follows:

$$\tau = \int_0^h k_\lambda(z)dz \tag{4.3}$$

This optical depth can be decomposed in the optical depth due to scattering (τ_s), cloud absorption (τ_c) and gaseous absorption (τ_g):

$$\tau = \tau_s + \tau_c + \tau_g \tag{4.4}$$

Shortwave radiative transfer in fog

The extinction of visible light under foggy conditions is a result of light absorption and scattering (Howell, Menguc, and Siegel 2015). The standard measure of visibility is the meteorological optical range (MOR), and is defined as the distance at which a luminous flux of a collimated light beam is reduced to 5% of its original value. The MOR $[m]$ can subsequently be calculated as follows (World Meteorological Organization 1983):

$$MOR = -\frac{ln(0.05)}{k_{\lambda vis}} \approx -\frac{3}{k_{\lambda vis}} \tag{4.5}$$

Where $k_{\lambda vis}$ is the extinction coefficient in the visible range.

The shortwave radiative transfer in fog is complex, as the radiative processes depend on radiation wavelength as well as the DSD of the fog. The total shortwave energy absorbed by fog is small and increases with liquid water content and under the presence of larger cloud droplets. The scattering of shortwave radiation also increases with liquid water content and depends strongly on wavelength and droplet size. For a given liquid water content, higher droplet concentrations and therefore smaller droplet sizes result in a higher single-scattering albedo (Cotton and van den Heever 2011).

The shortwave optical properties of fog are further complicated when ice crystals are present, due to uncertainties in ice crystal concentration and their size spectra. Furthermore, ice crystals are non-spherical and generally not randomly oriented in space. The transmission of shortwave radiation in an ice or mixed-phase cloud is therefore not only dependent on crystal size spectra, but also on spatial orientation and crystal geometry (Cotton and van den Heever 2011).

Longwave radiative transfer in fog

The interaction of longwave radiation with fog is quite different. While fog absorbs little shortwave radiation, longwave radiation can be strongly absorbed by fog with high liquid water content. In contrast, the magnitude of longwave radiation scattering is smaller. In comparison to a cloud-free atmosphere, the absorption of longwave radiation by fog is relatively constant with light wavelength. The absence of a distinct atmospheric window in a cloudy atmosphere can therefore strongly restrict the longwave emission to space. In contrast to the large dependence of the MOR on droplet size, the optical thickness for infrared wavelengths is largely a function of the liquid water content of a cloud and not dependent on its detailed DSD (Cotton and van den Heever 2011).

Optically thick clouds such as cumulonimbus clouds can be considered as blackbodies after a radiation pathlength of only 12m (Yamamoto, Tanaka, and Asano 1970), while the 'blackbody depth' of cirrus ice clouds may be several kilometers (Stephens 1983). As their vertical extent is smaller than that, they do not behave as a blackbody over the infrared range. Similarly, many fogs do not behave as blackbodies over the infrared range. The 'blackbody depth' of fog with respect to longwave radiation depends on its optical thickness and path length of the radiation.

The determination of a fog's optical thickness for longwave radiation is complicated by the fact that fogs with a similar MOR do not always have a similar relationship between the extinction coefficient and light wavelength. Fogs with a larger droplet size and higher liquid water content have a relatively larger extinction coefficient in the near-infrared range, compared to the visible range. In an observational study by Duthon et al. (2019), light radiative fog ($MOR > 100m$) was found to have a roughly constant extinction coefficient with light wavelength. However, for cases of very dense (MOR < 30 m) or advection fog, the attenuating impact of fog was about 10% higher in the near-infrared (1000 nm – 2400 nm)

range than in the visible (400 nm – 800 nm) range. The larger impact on higher wavelengths is a consequence of the larger droplet size and higher liquid water content in these kinds of fog.

The attenuation and emission of longwave radiation by fog can substantially affect the longwave radiative fluxes at the surface and fog top. The optical depth of shallow radiation fog is too small to significantly influence the longwave radiation budget. The presence of a deep fog layer can substantially increase the incoming longwave radiation at the surface, thereby redistributing part of the radiative cooling at the surface to the upper part of the fog layer. When the fog layer is some tens of meters thick, its optical thickness can be considerable and its upper part may become the effective longwave radiation emitter to space. Longwave radiative cooling at the fog top then leads to further growth of the fog layer and drives convection.

4.2.3 Thermodynamics in a foggy atmosphere

Differential extinction of radiation and thermal emission can change the internal temperature of an atmospheric layer. The net heating (or cooling) rate that results from radiative transfer processes is a function of the net radiative flux divergence F_N (Cotton and van den Heever 2011):

$$\frac{\partial \theta}{\partial t} = \frac{1}{\rho_0 C_p} \frac{\partial F_N}{\partial z} \tag{4.6}$$

Where θ is the potential temperature, ρ_0 and C_p are the density and specific heat of air respectively. For most cloud modelling applications the vertical radiative flux divergence is predominant and horizontal radiative fluxes can be neglected. F_N is then defined as the difference between upward and downward radiative fluxes integrated over all wavelengths (Cotton and van den Heever 2011):

$$F_N = F\downarrow - F\uparrow \tag{4.7}$$

When the incident energy flux and the scattered and transmitted energy in the system are not or only slowly changing, the amount of absorbed radiation is equal to the amount of emitted radiation. In conditions of local thermodynamic equilibrium the total emitted radiative flux of the atmosphere is given by:

$$F = \epsilon \sigma T^4 \tag{4.8}$$

Where ϵ represents the emittance of the atmosphere.

Fog evolution is strongly affected by three radiative processes that lead to heating or cooling of a fog layer. The first is the longwave cooling at Earth's surface and subsequently the fog top, resulting in condensation of new liquid water droplets. The second is the absorption of shortwave radiation by fog droplets causing heating of the fog layer and evaporation. The third process occurs when Earth's surface is warmer than the fog layer, due to absorption of shortwave radiation at the surface or substantial longwave cooling at the fog top. Sensible heat transfer from the surface to the fog can cause heating and evaporation of the fog from below.

In a stable boundary layer during the nighttime, $\frac{\partial F_N}{\partial z}$ is slightly negative due to radiative heat loss at Earth's surface. This condition is essential for (radiation) fog formation. When fog forms in an atmospheric layer, the emittance (ϵ) of the concerning layer directly increases. As a consequence, $\frac{\partial F_N}{\partial z}$ becomes negative leading to cooling of the layer, which subsequently leads to more condensation and thickening of the fog. The rate of cooling increases with the increasing liquid water content in the fog, until turbulent fluxes from Earth's surface start to compensate the radiative cooling.

Due to the increased incoming longwave radiation from the overlying fog layer, radiative heat loss at Earth's surface diminishes. When the fog thickens in the vertical, the top atmospheric layer that is filled with fog cools due to the radiative flux divergence. The radiative flux divergence in the lower atmospheric layer now becomes less negative, due to the increased incoming longwave radiation from the overlying fog layer. The radiative cooling thus continues at the fog top, and stagnates in the lower fog layers.

The effective emittance

The effective emittance is a commonly used quantity to express the combined effect of infrared reflection, emission and transmission from clouds. Usage of the effective emittance enables the deduction of IR cooling rate profiles in water clouds from broadband IR clear-air fluxes. The effective emittance is a directionally dependent vector as the emissivity depends on the path of radiation through the atmosphere. The upward and downward effective emissivity are defined following Kuhn (1963), and can be interpreted as the ratio of the divergence of observed directional irradiance to the directional irradiance if the fog

were a blackbody:

$$\epsilon(\uparrow) = \frac{F_B(\uparrow) - F_T(\uparrow)}{F_B(\uparrow) - \sigma {T_T}^4} \tag{4.9}$$

$$\epsilon(\downarrow) = \frac{F_B(\downarrow) - F_T(\downarrow)}{\sigma {T_B}^4 - F_T(\downarrow)} \tag{4.10}$$

Where $F(\uparrow)$ and $F(\downarrow)$ refer to the upward and downward irradiance, and subscripts T and B refer to the top and bottom of a cloud layer respectively. This definition neglects the effect of cloud reflectivity, which is a small percentage for IR wavelengths. The directional longwave radiation flux at any level z in the cloud is then given by:

$$F(\downarrow) = F_0(\downarrow) * [1 - \epsilon(\downarrow)(z)] + \epsilon(\downarrow)(z) * \sigma {T_B}^4(z) \tag{4.11}$$

5 Introduction to Harmonie

5.1 Background

In the past decades, most operational short-range Limited Area Models in Europe were developed by consortia of National Meteorological Services (NMS's). Two major collaborations are the HIRLAM (High Resolution Limited Area Model) consortium and the ALADIN (Aire Limitée Adaptation dynamique Développement InterNational) consortium. The HIRLAM consortium was established in 1985 and currently has members in NMS's of the following ten countries: Denmark, Estonia, Finland, Iceland, Ireland, Lithuania, the Netherlands, Norway, Spain and Sweden. The aim was to develop and maintain a numerical short-range weather forecasting system for operational use by its members. The collaboration resulted in the launch of the HIRLAM forecast system, which is used by member NMS's for routine weather prediction up to 72 hours at a grid resolution of 3 to 16 km. The ALADIN consortium was established in 1991 as a collaboration of 16 member NMS's from the following countries: Algeria, Austria, Belgium, Bulgaria, Croatia, the Czech Republic, France, Hungary, Morocco, Poland, Portugal, Romania, Slovakia, Slovenia, Tunisia, and Turkey.

In 2005, the HIRLAM consortium and ALADIN consortium decided to cooperate in a research project. The aim was to build a non-hydrostatic limited-area model code for short and very short range numerical weather forecasting. The model was named AROME (Applications of Research to Operations at Mesoscale). While the adiabatic part of the model is conform to the ALADIN code, AROME includes a different physics package adapted for the smaller grid resolution of around 2.5 km. The implementation and optimization to run AROME operationally within different European conditions required extensive adaptations and improvements in its physical parametrizations. This led to the development of two main model setups; a scripting system called HARMONIE-AROME (HIRLAM ALADIN Research on Meso-scale Operational NWP in Europe) and AROME-France. In 2014 the ALADIN and HIRLAM consortia agreed to merge their software with the objective to form a single, united consortium by 2020.

The website of the HIRLAM consortium (www.hirlam.org) provides further information on ALADIN, HIRLAM and associated research projects.

5.2 General description

HARMONIE-AROME (hereafter referred to as Harmonie) is currently the main operational weather forecast system at HIRLAM NMS's, among which KNMI since 2012. KNMI runs Harmonie version 40h1.1.1 every three hours, centered at Cabauw with a 2.5 km horizontal resolution. The model contains 65 vertical levels, the lowest level positioned at 12m AGL and the top level positioned at 10 hPa. The forecasting range is 48 hours, with an one-hour output interval resolution and a model time step of 75s. Initial profiles at the start of a model run are currently retrieved from the ECMWF global model, as well as lateral and model top boundary conditions in a data assimilation cycle during the run.

The adiabatic part of Harmonie is conform to the ALADIN code, based on the fully compressible Euler equations (Simmons and Burridge 1981). The evolution of the equations is realized by spatial and temporal discretization with a semi-Lagrangian advection scheme on an A grid and a semi-Implicit two-time-level scheme, both originating from the global Integrated Forecasting System (IFS) used operationally at ECMWF. Spectral representation of most prognostic variables is based on a double Fourier decomposition (Bengtsson et al. 2017). Sub-grid scale physical processes are resolved by parametrization schemes. This section contains an overview of the model physics that are relevant for fog formation and development. Furthermore, spatial and temporal model resolutions and the calculation of visibility by Harmonie are discussed.

5.3 Model physics

The description of model physics is restricted here to the key processes that are relevant for fog formation and development. These are:

- Radiation: Fluxes at cloud top (shortwave and longwave radiation), surface fluxes (shortwave and longwave radiation, heat, momentum and humidity)

- Cloud microphysics: Microphysical processes related to condensation and precipitation
- Turbulence: Turbulent eddy transports at cloud top
- Convection: Horizontal and vertical advection of heat and humidity
- Surface and soil processes: Heat and humidity fluxes

The combination of these processes and the model resolution determine the final quality of a fog simulation. Multiple sources that (might) limit the model performance have been reported, as well as various ideas for future strategies to improve the fog forecast (de Rooy 2014, Marthinsen 2015, Tijm 2019). Each section contains a general description of the concerned processes, and a summary of recent changes and relevant research outcomes that are related to fog simulation.

5.3.1 Radiation

The current scheme used for radiative transfer parametrization in Harmonie is a version of IFSRADIA, based on cycle 25R (ECMWF 2015b). The default shortwave (SW) radiation parameterization in IFSRADIA is the ECMWF Morcrette radiation scheme (IFS cycle 25R1), containing six spectral intervals between 0.185 and 4.00 μm. The default longwave (LW) radiation scheme in IFSRADIA uses the Rapid Radiative Transfer Model (RRTM) developed by Mlawer et al. (1997), and contains 16 spectral bands ranging from 3.33 to 1000 μm. A detailed description of both schemes can be found in ECWMF (2015b). In this thesis, the development of radiation fog during nighttime is researched. The shortwave radiation scheme is therefore not relevant and not discussed in detail.

The longwave radiation scheme

The RRTM longwave radiation scheme contains 16 spectral bands ranging from 3.33 to 1000 μm. Absorption coefficients for every spectral band are determined from the presence of active gases in the longwave spectrum. Longwave scattering is not taken into account. Downward fluxes of longwave radiation are calculated by vertical integration over every atmospheric layer, starting at the top of the atmosphere and going downward layer by layer. At the surface, the boundary condition is computed in terms of spectral emissivity and potential reflection of downward radiance. The upward radiance is then

calculated by the same vertical integration, starting at the surface and going upward. The spectrally averaged radiance $\bar{F}$ emerging from an atmospheric layer between wavenumbers ν_1 and ν_2 is:

$$\bar{F} = \frac{1}{\nu_1 - \nu_2} \int_{\nu_2}^{\nu_1} d\nu \left\{ F_0(\nu) + \int_{t_\nu}^{1} [B(\nu, T(t'_\nu)) - F_0(\nu)]\, dt' \right\} \tag{5.1}$$

Where $F_0(\nu)$ is the incoming radiance to the layer with wavenumber ν, $B(\nu, T)$ is the Planck function at wavenumber ν and temperature T, and t_ν and t'_ν are transmittances for the layer optical path and a point along this optical path respectively. A more detailed description of the RRTM longwave radiation scheme can be found in ECMWF-IFS (2016).

Full radiation calculations are performed every 15 minutes. The diagnostic output from the radiation schemes includes the accumulated spectrally averaged global downwelling SW flux, direct and direct normal surface irradiance. Net SW and LW radiative fluxes are provided on each model level, including the surface and top of the atmosphere. The downwelling diffuse SW radiation is calculated from the difference between the global downwelling SW radiation and the direct SW radiation at the surface. Both the direct SW flux and the diffuse SW flux include contributions from clouds as well as clear-sky components.

Clouds in the radiation scheme

Both the SW and LW radiative transfer equations use the inherent optical properties (optical thickness, single scattering albedo and asymmetry factor) of cloud particles, aerosols and atmospheric gases. Specific cloud liquid content, cloud ice content and H_2O are prognostic inputs. Monthly climatology values of aerosols and O_3 are used, and a fixed composition mixture of CO_2, N_2O, CH_4 and O_2. In each vertical column, a maximum-random cloud overlap is assumed.

The mean effective radius r_{eff} of the cloud water DSD is diagnosed from the cloud liquid water content L and the prescribed cloud condensation nuclei concentration (CCN) following the formulation of Martin et al. (1994):

$$r_{eff} = \left(\frac{3L(1+3d^2)^2}{4\pi\rho_w CCN(1+d^2)^3} \right)^{\frac{1}{3}} \tag{5.2}$$

where spectral dispersion $d = 0.43$ for continental air masses and $d = 0.33$ for maritime air masses. CCN is prescribed in Harmonie as 300 cm^{-3} for continental and 100 cm^{-3} for maritime air masses. Since the spatial and temporal variability in aerosol concentration is large, using constant values for CCN might cause some problems. As the impact of CCN concentrations on fog growth is large (Section 4.1), the influence of the prescribed CCN on the evolution of fog is researched in this thesis.

The effective dimension of ice cloud particles is parametrized following Sun and Rikus (2007) and Sun (2001).

The cloud optical depth in Harmonie is calculated following Smith and Shi (1990). A mass attenuation coefficient $\frac{\mu_{lw}}{\rho_m}$ is calculated from r_{eff}, in which μ_{lw} represents the attenuation coefficient for longwave radiation and ρ_m the mass density:

$$\frac{\mu_{lw}}{\rho_m} = 1.2 - 0.006 * r_{eff} \tag{5.3}$$

The liquid cloud optical depth τ_{cl} is then calculated from the liquid water path Lwp using a mass absorption coefficient for the total infrared flux a_{cl}, and diffusivity factor $\beta = 1.66$:

$$\tau_{cl} = \frac{a_{cl} * \frac{\mu_{lw}}{\rho_m}}{\beta} * Lwp \tag{5.4}$$

Diffusivity factor $\beta = 1.66$ accounts for the geometrical effect that longwave irradiance passes through clouds at an average cosine zenith angle assumed to be $\frac{1}{1.66}$. The total cloud optical depth τ_c is the sum of τ_{cl} and ice cloud optical depth τ_{ci} (τ_{ci} is not discussed in further detail here):

$$\tau_c = \tau_{cl} + \tau_{ci} \tag{5.5}$$

In Harmonie reference cycle 40h1.1, an uniform average value of $a_{cl} = 0.144$ is used for both upward and downward radiative fluxes, deviating from the method of Smith and Shi (1990). Smith and Shi (1990) propose to use independent emissivities for upward and downward radiation ($a_{cl}(\uparrow) = 0.130$, $a_{cl}(\downarrow = 0.158$), adopted from Stephens (1978). According to Stephens (1978), these directional dependent emissivities are required to account for the difference in spectral composition between upward and downward longwave beams incident on the cloud boundaries. These emissivities were determined from

a wide range of cloud types, using a multiple-scattering model in a standard U.S. atmosphere, and used to find an empirical relation between the effective emissivity ϵ (equation 4.10) and the liquid water path of a cloud layer. Least-squares fits were searched using the form:

$$\epsilon(\uparrow) = 1 - e^{(a_{cl}(\uparrow) * Lwp)} \tag{5.6}$$

$$\epsilon(\downarrow) = 1 - e^{(a_{cl}(\downarrow) * Lwp)} \tag{5.7}$$

Stephens (1978) repeated these calculations using moisture profiles based on tropical and subarctic winter atmospheres, and concluded that the downward emissivity is only lightly sensitive to changes in atmospheric temperature and moisture profiles. Sensitivity of the upward component was assumed similar. However, atmospheric changes since 1978, for example the decreased aerosol content, give rise to the question how representative the parametrization of a_{cl} is for our domain. The parametrization has furthermore not yet been validated in the Netherlands. The sensitivity of fog formation to a_{cl} is further researched in this thesis and compared to Cabauw measurements.

Since Harmonie reference cycle 40h1.1, two main changes have lead to a decrease in the downwelling SW flux under cloudy conditions. An improved cloud liquid optical property scheme for shortwave radiation is introduced, based on detailed Mie theory computations (Nielsen, Gleeson, and Rontu 2014). Furthermore, clouds are assumed homogeneous when present in a grid cell, contrary to a former inhomogeneity factor of 0.7 to account for cloud variability. This inhomogeinity factor β was formerly included to calculate an effective liquid water path Lwp_{eff} and an effective ice water path Iwp_{eff} (Tiedtke 1996):

$$Lwp_{eff} = \gamma * Lwp \tag{5.8}$$

$$Iwp_{eff} = \gamma * Iwp \tag{5.9}$$

Nielsen, Gleeson and Rontu (2014) criticized the usage of this inhomogeinity factor, as cloud transmittance and reflectance do not linearly depend on cloud optical depth. Instead, they proposed to use a more sophisticated optical property parameterization for liquid clouds and to set γ to 1.0. Furthermore γ was introduced before the transition to Harmonie in 2012, based on the 10-km horizontal resolution of Hirlam. Inhomogeinity is smaller in grid cells in Harmonie, due to the improved horizontal resolution to

2.5-km grid cells. Despite the lower SW budget under cloudy conditions, the total average SW budget has not changed due to a reduction in the overestimation of fog and low clouds as a consequence of stronger mixing in the boundary layer by a new turbulence scheme (section 5.3.3).

In Harmonie 40h1.1 the inhomogeneity factor γ has been set to 1.0, but no new parametrization for liquid clouds has yet been introduced. This might be a source of error, as the removal of the inhomogeneity factor leads to a larger impact of clouds on both the SW and LW radiation budget. Besides the reduced incoming SW radiation, the emission of LW radiation by clouds is increased leading to enhanced cooling of a cloud, and therefore increased persistence of clouds. The effect of the increased inhomogeneity factor on the longwave radiation scheme has not been tested so far. The usage of inhomogeinity factor $\gamma = 1.0$ is a second parametrization that is under research in this thesis.

5.3.2 Cloud microphysics

A one-moment bulk scheme is used to describe microphysics in Harmonie. It contains the three-class ice parametrization ICE3, which was originally developed for Meso-NH (Lascaux, Richard, and Pinty 2006). The following prognostic hydrometeors are included: cloud ice, snow, a variable combining graupel and hail, water vapor, cloud liquid water and rain. Horizontal advection is prescribed by a semi-Langrangian scheme, and vertical advection by a sedimentation scheme (Bouteloup, Seity, and Bazile 2011). Cloud fraction in three dimensions is determined using a statistical cloud and condensation scheme (Bechtold et al. 1995; Bougeault 1982). The autoconversion of cloud droplets to rain drops follows the "Kogan autoconversion" parametrization (Khairoutdinov et al. 2000).

In order to improve mixed-phase clouds under cold conditions, a recent update to the microphysical scheme has been made under the name "OCND2", described by Müller et al. (2017). Especially in the stable winter boundary layer, the original scheme often produced unrealistic low ice clouds. The original scheme was constructed to avoid supersaturation of water and ice. In clouds with temperatures between -5°C and -10°C, ice was generated too quickly, while in reality supercooled water droplets were present. Most supersaturation with respect to ice was removed when the temperature dropped below -20°C. Ice fog and ice clouds at the lowest level then formed, which were not observed. In reality supersaturation

under such conditions is realistic, due to the slow formation rate of ice clouds. The OCND2 treats the fraction of a grid box that is supercooled with respect to ice in a different scheme, such that the slower ice water processes are separated from the fast liquid processes. Other updates included in the OCND2 scheme are a reduction of the deposition rate of ice-phase water species, a correction of the cloud cover fraction to include the lower optical thickness of ice clouds compared to water clouds, and a reduction of ice nuclei concentration under freezing conditions.

The implementation of OCND2 reduces an existing negative bias of the 2m-temperature, reduces a dry bias in relative humidity in winter and improves low cloudiness in the lowest layers. A negative side-effect of these modifications is that that fog is overpredicted more frequently. Before the implementation of OCND2, this error was partly compensated by a too rapid precipitation release in the lowest layers.

5.3.3 Turbulence

A recent improvement in Harmonie Cy40h1.1 is the introduction of the HARATU (HARMONIE with RACMO Turbulence) turbulence scheme (Bengtsson et al. 2017). It is based on a scheme that was originally developed for the regional climate model RACMO (Lenderink and Holtslag 2004). The HARATU scheme uses a framework with a prognostic equation describing the turbulent kinetic energy (TKE) and a diagnostic length scale. Source and sink terms in the TKE equation include wind shear, buoyancy, transport and dissipation of TKE.

Condensation and evaporation of cloud droplets cause strong coupling between the turbulence scheme and the cloud and condensation scheme, due to the effect of latent heat on stability. Modelled fog fields are therefore quite sensitive to settings in the turbulence scheme (De Rooy 2014). Before the HARATU turbulence scheme was introduced, forecasted fog fields were frequently too dense and too persistent in Harmonie. The original CBR turbulence scheme was found to have to little cloud top entrainment, which provides the primary mechanism to dissolve a fog field (De Rooy 2014). HARATU has a larger cloud top entrainment, and produces better vertical profiles (e.g. wind, temperature and humidity profiles). Although the overprediction of fog and cloud cover was significantly reduced with the introduction of the HARATU scheme, fog is still too persistent in Harmonie (de Rooy and de Vries, 2017).

5.3.4 Convection

While deep convection is roughly resolved and explicitly represented by the nonhydrostatic dynamical core of Harmonie, shallow (sub-grid scale) convection is parametrized. Regarding fog forecasting, the main limiting factor is the 2.5-km model resolution as many sub-grid scale horizontal and vertical processes are relevant. Not many acute issues related to the convection scheme have been reported.

5.3.5 Surface and soil processes

Harmonie uses the externalized surface scheme SURFEX (Surface Externaliseé) to describe different surface types including soil, sea, inland water bodies and urban area database (Masson et al. 2003). SURFEX assumes a tile approach, such that the total surface flux of a grid box is calculated from the addition of the individual tile fluxes weighted by their respective fraction. Surface physiographies of the distinguished surface types are prescribed using the 1 km-resolution ECOCLIMAP database. The set of models that describe the different components in SURFEX can be found in the scientific SURFEX documentation.

Relevant to fog evolution is the surface boundary layer modeling scheme (SBL), which is a one-dimensional prognostic turbulence model. The exchange of energy and water between the atmosphere and surface types are herein computed, providing the lower boundary conditions for the lowest atmospheric model layer. The fluxes are computed as a function of the surface roughness, which is calculated from the leaf area index and vegetation height on land tiles. During an investigation to excessively persistent fog fields above the North sea and the Netherlands, de Rooy (2014) performed tests with different surface scheme options (ECUME, DIRECT, canopy scheme on/off), but observed no substantial impact on the formation of fog.

The 1D high resolution column model CANOPY has been used to calculate these fluxes until 2014 in Harmonie. When evaluating the performance of AROME-France, Donier et al. (2013) discovered an overestimation of summer nighttime T_{2m} as well as an underestimation of RH_{2m}. In these situations, the atmospheric stratification became too stable which was related to settings in CANOPY. The reduction of the maximum Richardson number Ri_{max} was reduced from 0.2 to 0.0 which lead to improved forecast

skill. CANOPY was switched off in Harmonie after 2014, as the usage of the CANOPY induced a large cold bias in dry and calm conditions (Driesenaar and Pottier 2014). Tijm and Diepenveen (2019) mentioned that Ri_{max} is still set to 0.0, and consequently the computed surface energy and water fluxes in stable boundary layers are based on a neutral boundary layer. Consequently, the exchange of these fluxes is larger than expected in a stable boundary layer, which promotes fog formation by too strong cooling of the lowest model layer. Tijm and Diepenveen (2019) showed that fog formation was reduced under increased Ri_{max}, particularly over urban area. The appropriate value of Ri_{max} is a third parametrization that is under research in this thesis.

5.4 Spatial and temporal model resolution

The current temporal resolution of 75 s is not expected to limit the models performance in fog forecasting. The current horizontal and vertical resolutions of Harmonie (2.5 x 2.5 km grid, and 65 height levels from which 9 in the lowest 200 m) are larger than the characteristic length and height scales of fog (100 m for the horizontal scale, a few meters for the vertical scale). Higher horizontal resolutions increase the skill in fog forecasting (Steeneveld, Ronda, and Holtslag 2015), but are computationally too expensive for operational usage. Grid nesting is often used to obtain increased detail in specific areas in a model. However, as this appears to disassemble the fog formation, Steeneveld, Ronda and Holtslag (2015) recommend to use a single domain and avoid the inclusion of nested domains.

Several studies have noted that a sufficiently high vertical resolution of numerical weather predicition models is important to solve the major processes related to fog evolution (Bergot et al. 2007). The development of radiation fog strongly depends on the vertical structure of the (nocturnal) boundary layer. A relatively fine resolution is required to adequately represent this structure and the strong vertical gradient at the fog top. Furthermore, as the lowest model layer in Harmonie is already 23.5 m thick, shallow fog layers can not exist and fog expands in large steps. The potentiality of a higher vertical resolution for operational usage equivalently depends on the possibility to increase computational capacity.

The introduction of increased detail can give insight to what extend fog forecast skill in Harmonie

	65 Layers			90 Layers		
n	**A(n)**	**B(n)**	**HAG [m]**	**A(n)**	**B(n)**	**HAG [m]**
0	0.000	0.998520	11.62	0.000	0.99407	4.65
1	0.000	0.995552	34.96	0.105	0.998014	15.59
2	0.000	0.992545	58.67	0.638	0.996206	29.76
3	0.000	0.989446	83.16	2.014	0.993990	47.11
4	0.337	0.986204	108.81	4.656	0.991372	67.56
5	1.768	0.982769	136.00	9.047	0.988358	91.07
6	4.875	0.979093	165.05	15.724	0.984952	117.54
7	10.019	0.975134	196.29	25.272	0.981161	146.95
8	17.661	0.970849	230.04	38.314	0.976989	179.21
9	28.366	0.966197	266.64	55.508	0.972441	214.27

Table 5.1: *Pressure constants $A(n)$ and $B(n)$ at model level n and winter average height above ground (HAG) of model level n.*

is limited by its resolution. A fourth subject of investigation in this research is therefore the impact of an increased vertical resolution of 90 layers on fog simulation in Harmonie, which might also be used in forthcoming versions of Harmonie. However, simply increasing horizontal and vertical resolutions in Harmonie without improving the parametrization could be the source of numerous problems. The current parametrizations of both ground and atmospheric processes are not adapted to a smaller scales, and therefore not accurate enough. Alhough parametrizations might not yet be optimal for a 90 layer resolution, the large gap between the characteristic vertical scale and the vertical model resolution gives ground to suspect that the error induced by suboptimal parametrizations might be smaller than the error due to a rough vertical scale.

Harmonie uses a hybrid hydrostatic pressure coordinate system to discretize the vertical coordinates in terms of pressure $P(n)$ based on pressure constant $A(n)$ at model level n, the fraction $B(n)$ of the

surface pressure P_s :

$$P(n) = A(n) + B(n) * P_s \tag{5.10}$$

$A(n)$, $B(n)$, the winter average layer height above ground and a winter average layer thickness for the lowest ten layers can be found in table 5.1 in case of both 65 and 90 vertical levels.

5.5 Computation of visibility in Harmonie

The MOR (equation 4.5) can be calculated once the extinction coefficient in the visible spectrum is known. An extinction coefficient in the visible spectrum in Harmonie is deduced from the Harmonie prognostic hydrometeors following Kunkel (1984). Empirical relations between the density of hydrometeors and a typical extinction coefficient for each hydrometeor are shown in table 5.2. A bulk extinction coefficient is then calculated as the sum of the extinction coefficient of each hydrometeor, plus a constant background extinction coefficient k_b which represents the extinction due to air molecules and a fixed background aerosol concentration:

$$k = k_{clw} + k_r + k_{ci} + k_s + k_g + k_b \tag{5.11}$$

In contrast to the definition of the MOR by the WMO (2008), the standard MOR in Harmonie is defined based on a light beam reduction to 2% of its original value. This results in a 30% larger MOR than when the standard contrast threshold of 5% is used. Consequently, the MOR is calculated as follows:

$$MOR = -\frac{ln(0.02)}{k} = -\frac{ln(0.02)}{144.7W_{clw}^{0.88} + 1.1W_r^{0.75} + 163.9W_{ci}^{1.00} + 10.4W_s^{0.78} + 2.6W_g^{0.78} + k_b} \tag{5.12}$$

Equation 5.12 contains an empirical relation between the MOR and hydrometeor densities. As visibility is strongly dependent on the DSD of a fog, the uncertainty in deducing visibility during foggy weather is large. The usage of a monthly climatology for aerosol concentration introduces a supplementary source of error, as the variability in aerosol concentration is large (Marthinsen 2015). A third complication is that visibility is an integral measurement that represents a large area, while total cloud water represents the average over a grid cell. Actual visibility in a grid cell does therefore depend on the neighbouring grid cells.

Hydrometeor	Extinction coefficient
Cloud Liquid Water	$k_{clw} = 144.7 W_{clw}^{0.88}$
Rain	$k_r = 1.1 W_r^{0.75}$
Cloud Ice	$k_{ci} = 163.9 W_{ci}^{1.00}$
Snow	$k_s = 10.4 W_s^{0.78}$
Graupel	$k_g = 2.6 W_g^{0.78}$

Table 5.2: *Extinction coëfficients for the different hydrometeors in Harmonie. W represents the density of the hydrometeor in* $\frac{g}{m^3}$.

The diagnostic formulation of visibility based on the Kunkel parametrizations has shown to give too high visibility in aerosol-dense air in China, while the predicted visibility in Northern Europe is too low. The Kunkel relations were derived based on observations in the North-East USA in 1980. As discussed in section 4.1, air in present-day Northern Europe is cleaner. The MOR calculated by the Kunkel relations is therefore presumably too low. Equation 5.12 is therefore used in this thesis only to give a rough approximation on the visibility impact of fog. Otherwise, the 'thickness' of fog is evaluated in terms of liquid cloud water concentration.

6 Introduction to Cabauw

Since 1973, the Cabauw Experimental Site for Atmospheric Research (Cesar) has been a major source of atmospheric measurements in the Netherlands. The consortium involves eight institutes and universities in the Netherlands, and provides remote sensing and in-situ routine measurements form the Cesar site. Collected observational data includes information on the state of the atmosphere, its radiative properties and land-atmosphere interactions.

The Cesar site (51°58′12.00″N, 4°55′34.48″E) is located near Cabauw, in a polder 0.7m BSL in the western part of the Netherlands. Topographical influences are negligible as the Cesar site is located in a flat polder mainly surrounded by grassland. Profile observations of high resolution have been carried out since 1972 with the 213 m high Cabauw tower, providing useful data to investigate boundary layer meteorology.

In this thesis, micrometeorological routine observations from the Cesar Observatory are used to investigate and illustrate the interaction between synoptic thermodynamic and dynamical factors and fog. The relevant measurements are the surface air pressure, surface budgets of radiation, heat, water and momentum and profile observations of wind speed, wind direction, temperature, dew point temperature and visibility. For a more detailed description on the instruments, calibrations and set-up of the Cabauw observational program, the reader is referred to Bosveld (2019).

6.1 Surface observations

The Cesar dataset provides surface observations of air pressure, and surface budgets of radiation, heat, water and momentum averaged on a 10 minute time interval. Surface air pressure is measured using a Paroscientific 1016B-01 on the 10 m windmast of the automatic weather station 200 m south of the main tower, with an accuracy of 0.1 hPa.

Surface budgets of longwave and shortwave upward and downward radiation are measured at Cabauw

at 1.5 m height with Kipp&Zn CM22 pyranometers. The surface soil heat flux G is derived from a combination of observations with soil heat flux plates and soil temperature needles. Vertical fluxes of momentum and sensible heat (SH) are derived from a combination of measurements with a sonic anemometer/thermometer and an optical open path sensor. The latent heat flux LH is then calculated from the total surface radiation budget Q_n, SH and G following the surface energy balance:

$$LH = Q_n - SH - G \tag{6.1}$$

The uncertainty in the calculated LH is thus relatively large, due to the propagation of errors in the experimental measurements of Q_n, SH and G. Rain amount and duration are observed at the meteo-field south of the main tower. Rain amount is directly measured with the KNMI rain gauge, and rain duration is derived from these observations. Other precipitation types are not in the scope of this thesis, as only foggy weather with air temperatures above freezing is analyzed.

6.2 Tower observations

The Cesar dataset provides profile observations of wind speed, wind direction, temperature, dew point temperature and visibility from the Cabauw tower, averaged on a 10 minute time interval, measured at seven levels between 2 and 200m (2m, 10m, 20m, 40m, 80m, 140m and 200m).

Wind speed and wind direction are measured at six levels between 10 and 200 m. Wind speed is measured with the KNMI cup-anemometer. Wind direction is measured with the KNMI wind vane in an angle resolution of 1.5°. Wind speed and wind direction are measured at different positions along the Cabauw tower, to avoid flow obstruction from the mast and the main building. For each 10 minute interval, the instruments that are best exposed to the wind are selected.

Air temperature is measured at eight levels between 0.1 and 200 m. Dew point temperature is measured at seven levels between 2 and 200 m. Both are measured in one unventilated hut, consisting of two compartments on top of each other. The lower compartment contains a EPLUSE Pt1000 element that measures air temperature, the upper compartment contains a heated EPLUSE 33 polymer sensor

that measures dew point temperature. As vertical gradients close to the surface can be significant over the depth of the hut, surface instruments for air temperature and dew point temperature are located in separate huts at the same level. Profile observations of specific humidity are derived from dew point temperature and air pressure.

Visibility is measured at seven levels between 2 and 200 m since 2011. At the 2-m level, visibility is measured with a Vaisala FD12P weather sensor, with a maximum detectable visibility of 50 km. Observations at higher levels are done with light scattering sensors of type Biral SWS-100, with a maximum range of 20km. During a fog event all sensors up to a certain level should indicate low (<1 km) visibility.

In the past years several experiments were carried out with the Cabauw tower, among which the installation of a ventilated and heated Kipp&Zn CM22 pyranometer at the top of the tower (213 m), to measure downward radiative fluxes for a fog observational program. Combined with routine surface radiative fluxes and the temperature profile, the effective emissivity of the atmosphere between 200 and 2 m can directly be calculated from these measurements.

7 Methods

7.1 General outline

To obtain further insight in the evolution of fog in Harmonie, a case study is selected in which radiation fog is overestimated by Harmonie. The evolution of the fog layer is compared to measurements from the Cabauw tower at the corresponding date. The selected case is the night of 28/29 March 2019, when fog in Harmonie expanded to a maximum thickness of 80 m, while Cabauw visibility measurements indicate a maximum fog thickness of only 20 m. After analysis of this fog case, the 1D model MUSC is used for testing the performance of new parametrizations that sharpen the physical correctness of the model and therefore might improve the quality of fog forecasts. The new parametrizations are defined empirically, based on Cabauw measurements of radiation fog events between October 2012 and March 2019. After selection of the best performing parameter settings, the Harmonie run at 28/29 March is repeated for evaluation.

This chapter contains an overview of the used data from Harmonie and from the Cesar observatory, as well as a description how these datasets are compared. Furtermore, an introduction to MUSC is given, with an outline how MUSC is used to contribute to improvement of Harmonie.

7.2 Comparing Harmonie to Cabauw

Harmonie produces a 48 hour forecast every three hours, and different runs are available: two operational runs at KNMI (cycle 36 for operational usage and cycle 40h1.1.1 parallel), two runs with 65 levels at the ECMWF (Harmonie 40h1.1.1 and 43h2.1 target 1) and one run at the ECMWF with 90 levels (Harmonie 43h2.1 target 1). Multiple forecasts are therefore available for every given time. The selected forecast to evaluate the performance of Harmonie is the ECMWF cycle 40h1.1.1 run of 28 March 2019 12:00 p.m. (UTC+1) with the standard vertical resolution of 65 pressure-based hybrid levels. This run is

repeated with an increased vertical resolution of 90 layers, to evaluate the impact of increased detail in the lowest layers. Both runs are compared to each-other and to measurements from the Cabauw tower. The Cabauw tower data is freely accessible from the Cesar Database webportal. To evaluate the performance of Harmonie, the Harmonie runs are compared to Cabauw data from the night of 28/29 March. Furthermore, Cabauw observations of 162 nighttime radiation fog cases between October 2012 and March 2019 are used to evaluate the physical correctness of Harmonie model settings. In this way a broader picture is sketched to recognize unusual behavior during fog episodes in Harmonie, which is particularly useful where the Harmonie forecasts deviate largely from the Cabauw observations during 28/29 March 2019.

To compare the evolution of fog in Harmonie to Cabauw measurements, a primary parameter must be selected that indicates the presence of fog, as well as key parameters that describe its physical properties. An important complication here is that there is a mismatch between parameters that are available from Cabauw measurements and from Harmonie simulations. While the presence of fog is measured at the Cabauw tower in terms of visibility, this is no direct output from the Harmonie model. The presence of fog in the Harmonie model can be deduced from the amount of cloud water and cloud ice, that are calculated in the microphysical scheme. A standard method exists to calculate visibility from cloud water and ice content (section 5.5). However, this method relies on many assumptions that are under discussion, regarding aerosol content and the optical properties of fog in the shortwave spectrum.

Equation 5.12 is used here to determine what concentration of cloud water indicates the presence of fog in Harmonie. Cloud ice was not present during 28/29 March 2019. In contrast to the standard MOR calculations in Harmonie with a contrast threshold of 2%, a contrast threshold of 5% is used as defined by the WMO (2008) for consistency with Cabauw observations. Fog in Harmonie is then present at a minimum cloud water concentration W_{cl} of:

$$W_{cl,fog} = 0.0122 - k_b \approx 0.0120 \; [\frac{g}{kg}] \tag{7.1}$$

Furthermore, equation 5.12 is used to roughly compare the MOR of fog in Harmonie to the MOR measured at Cabauw, with the sidenote that the conversion of cloud water and ice to visibility introduces

a large source of uncertainty.

Additionally, parameters are compared that have key roles in fog evolution and that reflect the physical properties of fog. As the characteristics of the surface air layer are critical for the development of radiation fog, budgets of specific humidity and wind speed in this layer are compared. For consistency, measured and forecasted parameters are compared in a layer thickness of 23 m, which is (roughly) the thickness of the lowest Harmonie-65l layer. For both the Harmonie-90l forecasts as well as Cabauw measurements, the value of parameters in a 23 m thick layer are computed as a weighted average of the standard output layers.

Furthermore, temperature, latent and sensible heat, radiation budgets and precipitation during the fog case are compared, and different hypotheses on the origin of erroneous fog representation in Harmonie are formed. These hypotheses are subsequently tested using the 1d-model MUSC and by full compilation of Harmonie.

7.3 Introduction to Musc

MUSC (Modèle Unifié Simple Colonne, hereafter referred to as Musc) is a single column version of Harmonie based on the work of Malardel et al (2006). In this thesis, Musc experiments based on code from Harmonie cycle 43h1 are performed to explore the nature of the erroneous fog forecasting in Harmonie. Musc is quick to compile and run, as all physical processes are run in a vertical column of four grid cells. Musc is therefore a helpful tool to study the behavior of a simulated fog layer, and useful for testing the performance of new parametrizations.

Physical processes in Musc are driven by large scale forcings provided by Harmonie. The initial atmospheric state and near-surface properties of experiments in this thesis were extracted from the 9:00 p.m. output of 3D Harmonie runs of 28 March 2019 initialized at 12:00 (UTC). All experiments are performed at the standard vertical resolution of 65 levels, and with an increased vertical resolution of 90 levels. The surface temperature in the initial atmospheric states was slightly lowered, to create a fog layer that starts forming at the lowest model level and then expands in the vertical. The step-wise

growth of the fog layer in the vertical provides a basic setting in which the interaction of different physical properties of the fog can be studied. To study the fog evolution in more detail, the timestep in Musc is decreased to 6 seconds, with an output resolution of 60 seconds.

Although initial conditions at 9:00 p.m. are similar in the Harmonie case study and the Musc experiments, several factors complicate the direct comparison between these two. Firstly, there are revisions in several model parts that have been implemented in Harmonie cycle 43. The setup of Musc therefore differs slightly from Harmonie cycle 40. Also, the adaptation of 3-dimensional processes to a vertical column causes different fog behavior. An example is the absence of (weak) advection in Musc, which enables the outflow of fog to neighbouring grid cells. Musc is therefore only used for testing the performance of new parametrizations by comparison of output changes to output of Musc reference experiments, and not to compare the outcome of experiments directly to Harmonie output. In this way, parametrizations are identified that have the potential to improve the performance of Harmonie.

Several Musc experiments are performed to explore causes and consequences of the deviant fog behavior in Harmonie. The choice for this set of experiments follows from results that are found in the Harmonie fog case study, and are elucidated more explicitly in section 9. An experiment overview is summarized here:

- Reference experiments with the original settings run over 65 and 90 layers.
- Experiments with reduced longwave emissivity to 70%, 50%, 25% and 10% of its original value in the reference experiments. This includes experiments with reduced mass absorption coëfficient a_{cl} from 0.144 to 0.096 and experiments with reduced inhomogeinity factor γ from 1.0 to 0.7.
- Experiments with increased maximum Richardson number Ri_{max} from 0.0 to 0.2 and 1.0.
- Experiments using the radiation scheme Acraneb instead of RRTM.
- Experiments with reduced CCN from 300 cm^{-3} over land and 100 cm^{-3} over sea to 50, 25 and 10 cm^{-3} for both sea and land.
- Experiments in which these adapted parametrizations are combined.

When errors or sensitivities are found that cause changes in the fog development in Harmonie that

reduce the systematic errors related to fog simulation, the proposed model adaptations are also tested in 3-d Harmonie Cy43h2.1 (target 1) experiments.

7.4 Comparing Harmonie Cy43 to Harmonie Cy40

While Harmonie Cy40h1.1.1 is currently operationally run at KNMI, the target model cycle is Harmonie Cy43h2.1 (target 1) as KNMI will switch to this cycle in the future. The experiments with proposed model adaptations are therefore run with Harmonie Cy43, as well as a new reference experiment with 65 layers. An overview of main differences between both versions that are relevant to fog simulation is given in this section.

Three updates in the development of Harmonie Cy43 are associated with soil and surface processes. The first is the substitution of the surface database ECOCLIMAP 2.2. by ECOCLIMAP Second Generation, which is more accurate in describing the yearly cycle of the leaf area index. Furthermore, the resistance of stomata against evaporation is increased, and the adjustment of surface moisture by data assimilation is reduced. With these changes, the amount of evaporation is reduced, which was overestimated especially in spring in Harmonie Cy40. A side effect of the updates to the SURFEX scheme is a reduction of the surface roughness, which is not yet validated. Regarding atmospheric processes, the mixing of free atmosphere is reduced in Harmonie Cy43, which improves the skill in simulation of low clouds. Additionally, a new statistical cloud scheme is implemented, and an option to use height-dependent aerosol concentrations is included.

8 A FOG CASE STUDY

An interesting case when fog was overpredicted by Harmonie is the night of 28/29 March 2019. A KNMI analysis of the background meteorological conditions in the surrounding environment in the night of 28/29 March is shown in figure 8.1. Except a cold front over the central parts of Scotland and Northern Ireland bringing drizzly rain followed by moderate showers, most locations in Northwestern Europe were calm and dry at midnight. A stable high-pressure system covered the Netherlands and the North Sea, creating a setting during this night that was typically favorable for radiation fog to develop; a clear and cloudless sky, moist air and Southwestern surface wind speeds varying between 0.5 and 2.0 $\frac{m}{s}$. Shortly after sunset, a shallow radiation fog layer developed over the Netherlands. Harmonie simulations overestimated this fog event in cloud water density as well as horizontal and vertical expansion. Many aspects of the behavior of this fog layer in Harmonie are different from the fog layer that was observed at Cabauw. These differences are analyzed and discussed in this section, to hypothesize on possible sources of the divergent fog behavior in Harmonie.

Figure 8.2 shows the evolution of the fog event during 28/29 March simulated by Harmonie. After sunset, the fog initializes in distinctive patches over land, that gradually expand to form a contiguous layer of thick fog that covers both the western Netherlands and part of the North sea. After sunrise, the fog layer starts to dissolve to ultimately disappear over the land, while the fog over sea persists longer. From satellite observations (figure 8.3), it is clearly visible that such extensive horizontal fog expansion did not occur in reality. The shallow layer of radiation fog formed similarly but only developed into a shallow light layer, and with exception of a small area in the Northwestern part of the Netherlands all fog had already disappeared at 07:00 A.M.

Liquid water concentration from Harmonie and the MOR measurements at Cabauw are displayed in figure 8.4 and figure 8.6A. In the Cabauw observations, a shallow fog layer forms shortly after sunset. The MOR at 2 m fluctuates around 200 m during the night. After midnight, the MOR at 10 m and subsequently the MOR at 20 m drops to values between 120 and 350 m, having a sharply fluctuating

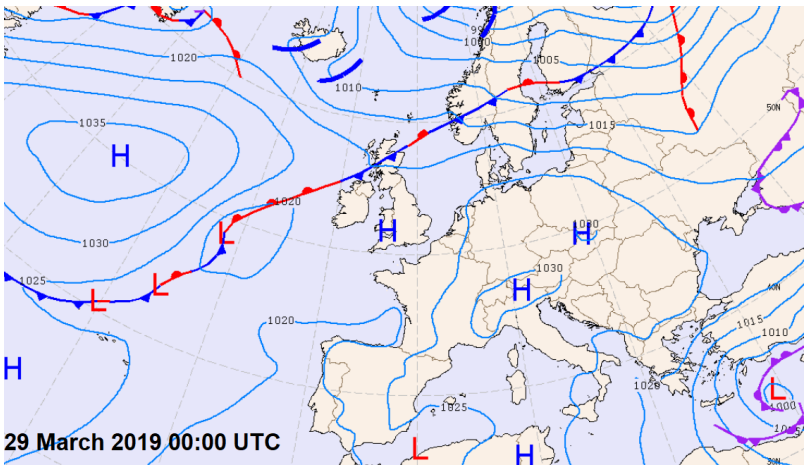

Figure 8.1: *Weather analysis of 30 March 2019 00:00 UTC by KNMI, based on HIRLAM. Adopted from KNMI-Weerkaarten Archief Europa.*

character. The MOR at 80 m is fairly low (3000 m) after 02:00 AM. This may indicate the presence of a very thin low stratus layer, but more probably it shows a measurement error due to a contaminated visibility sensor as no cloud cover is observed in satellite images and the relative humidity at this time and height and was only 70%. After the fog has reached its maximum thickness of 20 m, it dissipates after sunrise. The fog layer has no observable impact on the longwave radiation budget (figure 8.6C), and the atmosphere is dominantly cooled from below. Net condensation of dew at the surface is deduced from the latent heat flux (on average 19.7 $\frac{Watt}{m^2}$, figure 8.6E) and amounts to 0.031 $\frac{mm}{hour}$.

In contrast, Harmonie forecasted a fog layer that forms at 01:00 AM and gradually grows until it reaches a maximum thickness of 96.5 m (65 levels) and 105.5 m (90 levels) at 10:00 AM, where after it dissipates. The temperature in the lowest model layers strongly reacts to the presence of fog (figure 8.5, figure 8.6D). After the entrance of fog in a model layer, this layer is cooling quickly (a few degrees in one hour), thereby replacing part of the radiative cooling at the surface to the fog top. For example, in figure 8.5A at 04:00 A.M, fog enters L1 (layer numbers are given in table 5.1) and the temperature in this layer subsequently drops by 6 K from 280 to 274 K. This indicates a radiative flux divergence

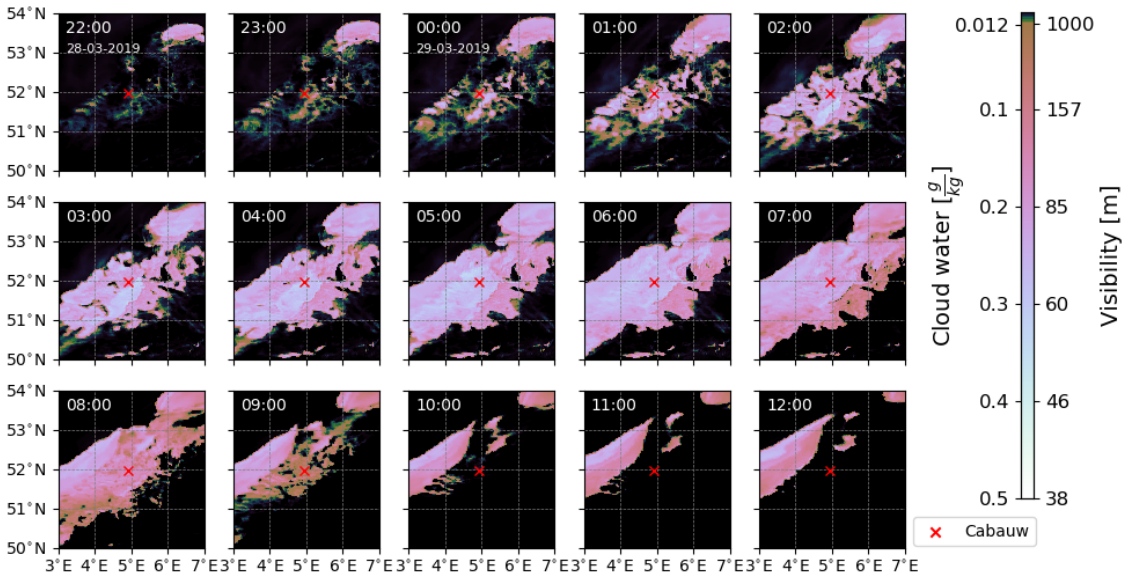

Figure 8.2: *Cloud water forecast by Harmonie Cy40 at vertical level L0, using a vertical resolution of 65 layers.*

of about $\frac{23m^3 * 1.2\frac{kg}{m^3} * 6K * 1000\frac{J}{kg*K}}{3600\frac{s}{hr}} = 46\frac{W}{m^2}$ (the vertical thickness of L1 is 23 m), meaning that the layer has an absorption coefficient close to 1. The temperature in the fog is consequently much lower than the temperature measured at Cabauw. When this temperature drops below the surface temperature, sensible heat transfer from the surface to the fog causes heating and evaporation of the fog from below (figure 8.6F). In Cabauw, this only happens after sunrise when Earth's surface warms by shortwave absorption.

The fog forecasted by Harmonie becomes remarkably dense. Although the comparison of visibility from Cabauw and cloud water from Harmonie is questionable due to the uncertain conversion between the two, forecasted fog by Harmonie is certainly denser as the maximum LWC rises to 0.36 and 0.37 $\frac{g}{kg}$ for 65 and 90 layers respectively. Using equation 5.12, this corresponds to a MOR of 50 m, while the minimum MOR observed at Cabauw was 120 m (LWC=0.16 $\frac{g}{kg}$). As liquid water content in observed fog is rarely higher than 0.2 $\frac{g}{kg}$ (section 4.1), the physical correctness of the high liquid water content

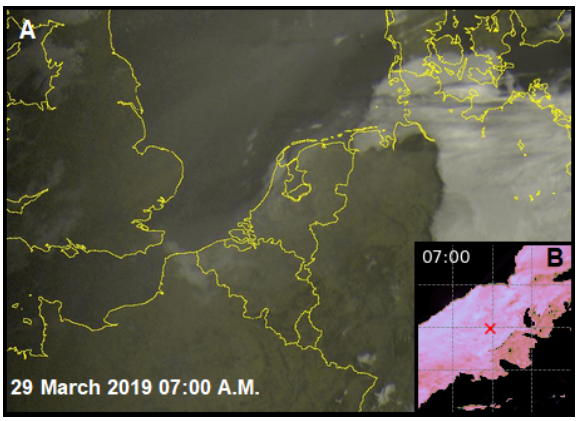

Figure 8.3: *(A) Visible satellite image of the Netherlands at 30 March 07:00 A.M (UTC) compared to (B) Harmonie forecast as in figure 8.2 at the same time. Radar image was adopted from Buienradar-Satellite Archive Europe.*

forecasted by Harmonie is highly questionable.

In contrast to Cabauw, the latent heat flux in Harmonie is close to 0 during the night. This difference in air moisture loss is partly compensated by slight rain formation in Harmonie (up to 0.024 $\frac{mm}{hr}$), while no rain is observed at Cabauw during the night (figure 8.6G). The difference in the latent heat flux may be a consequence of overestimating evaporation or underestimating dew formation in Harmonie, but as the latent heat flux at Cabauw closes the energy balance (equation 6.1) this difference may also reflect measurement errors.

To summarize, in both Harmonie forecasts a fog layer develops that becomes too dense, too cold and too optically thick for longwave radiation. These characteristics give insight in what direction to search, however it is not yet possible to identify cause and consequence. The longwave radiation scheme may be too sensitive for cloud water (and maybe also cloud ice); if the emissivity of the fog layer in the model is too large, the layer cools too quickly resulting in too extensive fog growth. On the other hand, the microphysical scheme might be too sensitive for radiative cooling. If cloud water condenses too fast in a cooling layer, the radiative cooling increases too fast resulting in enhanced fog growth. A third cause

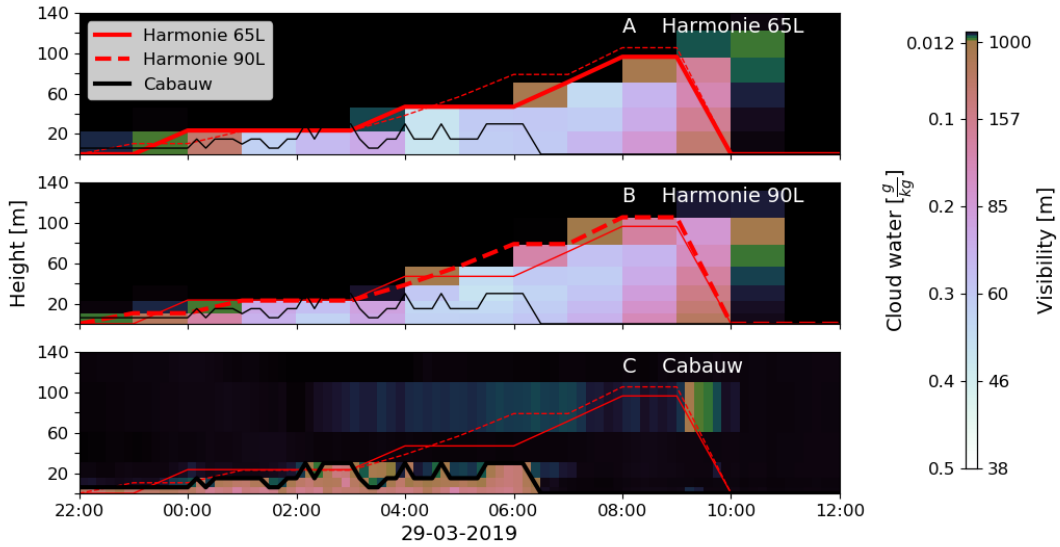

Figure 8.4: *(A, B) Cloud water forecasts by Harmonie Cy40 using a vertical resolution of (A) 65 layers and (B) 90 layers. (C) Visibility observations at Cabauw. Contours are drawn where fog is present (MOR<1000m at all levels from surface upwards).*

might be found in the surface scheme of Harmonie. If the rate of dew condensation and precipitation is too low, a too large proportion of the excess water vapour condenses into fog when the air temperature drops. The origin of the overestimation of fog is studied in more detail in Chapter 9 by the evaluation of various Musc experiments.

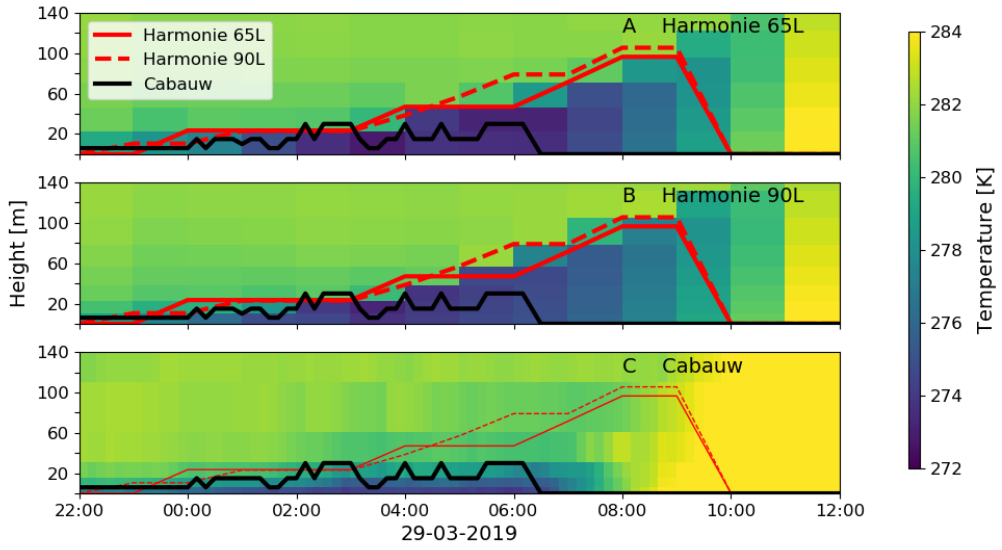

Figure 8.5: *(A, B) Air temperature forecasts by Harmonie using a vertical resolution of (A) 65 layers and (B) 90 layers. (C) Air temperature observations at Cabauw. Contours are drawn where fog is present (MOR<1000m at all levels from the surface upwards).*

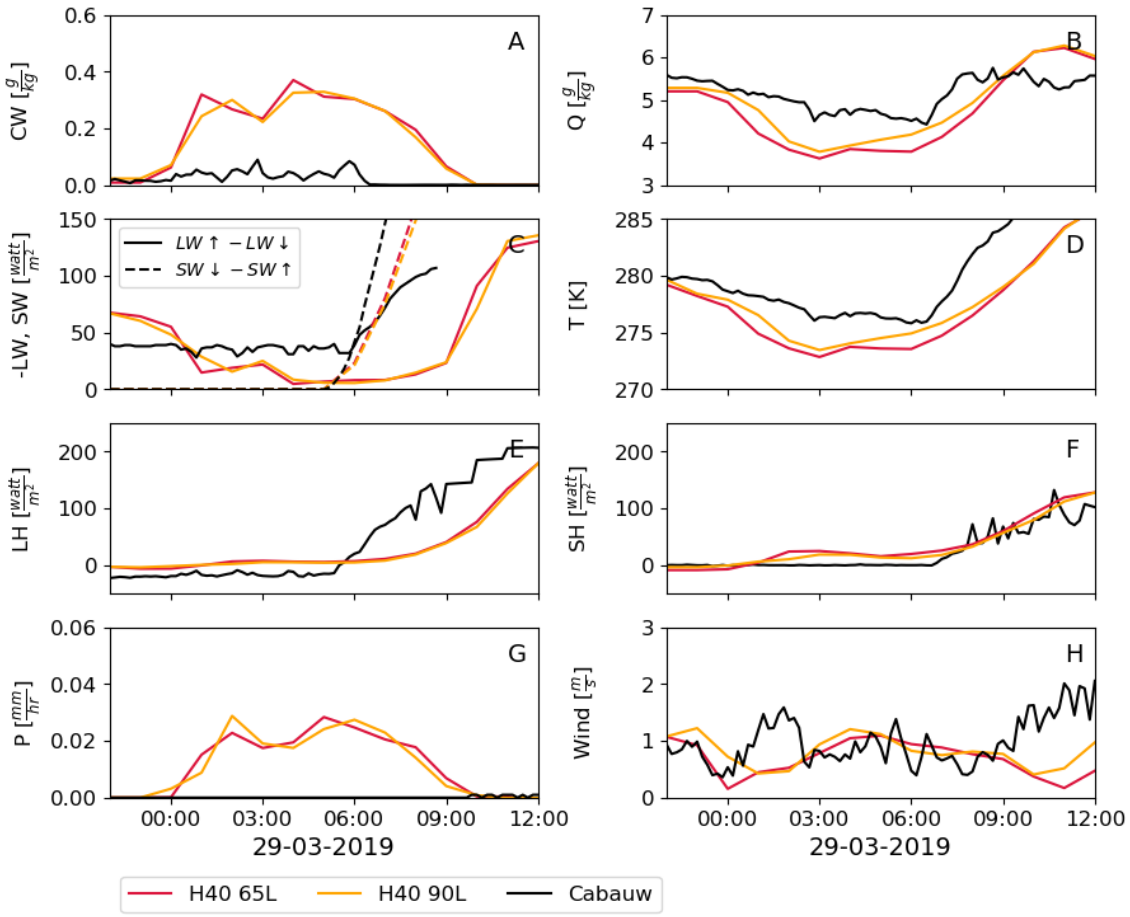

Figure 8.6: *Harmonie forecasts and Cabauw observations during 28/29 March 2019. (A) Average cloud water in the lowest 23m-thick atmospheric layer L0 (note: observed cloud water was deduced from Cabauw MOR observations). (B) Average specific humidity in the lowest 23m-thick atmospheric layer. (C) Net outgoing longwave radiation and net incoming shortwave radiation at Earth's surface. (D) Temperature in L0. (E) Latent heat flux at Earth's surface, positive when heat is transported away from the surface. (F) Sensible heat flux at Earth's surface, positive when heat is transported away from the surface. (G) Total precipitation at Earth's surface. (H) Average wind speed in L0. H40 65L and H40 90L refer to Harmonie Cy40h1.1.1. forecasts with vertical resolutions of 65 layers and 90 layers respectively.*

9 Testing with Musc

9.1 Reference experiments

The reference experiments are configured as described in section 7.3 and used to study the current fog behavior in Harmonie in more detail with a temporal output resolution of 60 s. The reference experiments have vertical resolutions of 65 and 90 layers, and are hereafter referred to as Ref-65L and Ref-90L respectively.

The evolution of liquid water concentration in the reference experiments is displayed in figure 9.1. In Ref-65L, the fog layer starts to form at 00:00 P.M and reaches a maximum vertical height of 122 m at 09:00 P.M. When the vertical resolution is increased to 90 layers, the fog emerges two hours earlier and grows slightly higher with a maximum thickness of 132.5 m. The maximum cloud water concentration is highest in model layers between 40 and 70 m, and increases to 0.48 and 0.44 $\frac{g}{kg}$ for 65 and 90 layers

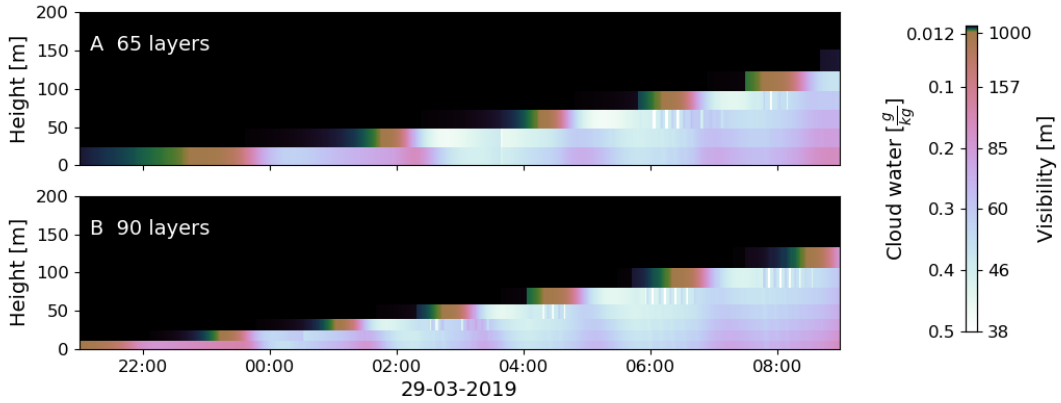

Figure 9.1: *Cloud water forecasts by Musc using a vertical resolution of (a) 65 layers and (b) 90 layers.*

respectively. Both the vertical extension and concentration of the fog is therefore larger in the Musc experiments than in the Harmonie fog case study of 28/29 March 2019, while initial conditions (at 9:00 PM) and boundary conditions are similar.

Similar to the Harmonie case study, the layer temperature is prominently correlated to the presence of fog (figure 9.4A, B), dropping by 4.2 K (65 levels) and 5.9 K (90 levels) respectively. The increased resolution therefore seems to promote longwave cooling and further growth of the fog. The correlation between longwave cooling and the cloud water content of fog is presented with more detail in figure 9.5A, B. The temperature decrease during the initial formation of fog in a layer follows a clearly distinguishable path. This direct correlation holds until fog starts to form in an overlying model layer that causes an increase in the downward longwave radiation flux that is transferred from the overlying layer towards the layer. While the total cooling and maximum cloud water content is independent of layer level between L1 and L9 for Ref-65L, these increase with layer height for Ref-90L. This is a consequence of the smaller layer thickness, decreasing the time that a fog forming layer is emitting with maximum efficiency due to fog initialisation in the overlying layer. Higher layers are vertically thicker, consequently these are longer positioned at the fog top where infrared cooling is strongest.

The impact of the fog on the radiation budgets at Earth's surface is displayed in figure 9.6E (Ref-65L) and figure 9.6F (Ref-90L). Figure 9.6E shows that the increase in downward longwave radiation due to the entrance of fog in L0 causes a net reduction of 48 $\frac{watt}{m^2}$ in the net longwave radiation budget. In case of 90 levels, the entrance of fog in L0 only induces the longwave budget to drop by 23 $\frac{watt}{m^2}$, and the entrance of fog in L1 is responsible for another reduction of 30 $\frac{watt}{m^2}$. Consequently, while the the temperature in L0 drops very fast as the fog layer directly starts to emit (figure 9.6I), it decreases more gradually in Ref-90L (figure 9.6J). The increased resolution causes the evolution of forecasted parameters therefore to smoothen. Although the behavior of the fog in Ref-65L causes more bumpy behavior of the forecasted parameters, the skill in fog forecasting is not improved in Musc when the vertical resolution is increased as it grows thicker and cools faster.

9.2 Testing longwave emissivity

A possible explanation for the quick cooling of the fog layer is a too large sensitivity of the longwave radiation scheme to the presence of water droplets. In section 5.3.1 the interaction of longwave radiation with a cloud layer in Harmonie is discussed in detail. Two main causes are identified here that support the suggestion that the current optical depth to longwave radiation τ_{cl} in Harmonie is too high. The longwave effective emissivity a_{cl} that was adopted from Stephens (1978) may be too large, as it was determined in 1978, before the reduction in aerosol emissions that is correlated to a decrease in dense fog events over the Netherlands. Furthermore, the introduction of the increased inhomogeinity factor $\gamma = 1.0$ in 2014 may be inaccurate for longwave radiation. In this section, the validity and usage of a reduced value of τ_{cl} is examined by deriving an up-to-date parametrization of ϵ based on the Cabauw database as well as evaluation of Musc experiments with lowered τ_{cl}.

The measurement of downward radiative fluxes at the top of the Cabauw tower and the surface enables the deduction of longwave effective emissivity during foggy weather. Using equation 4.10, the effective emissivity for longwave radiation is calculated from nighttime Cabauw measurements during fog events

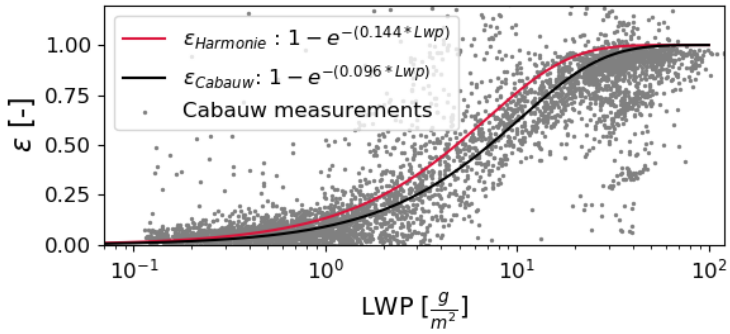

Figure 9.2: *Empirical presentation of effective emissivity ϵ as a function of liquid water path. The red curve represents the emperical relation that is currently used in Harmonie. The black curve is a least squares best fit through the Cabauw measurements (grey dots).*

between October 2012 and March 2019. These measurements are plotted against the liquid water path (figure 9.2), that was deduced from Cabauw MOR measurements by using equation 5.12 and vertical integration. A least squares best fit through these data points resembling equation 5.7 indicates an optimal value for mass absorption coefficient $a_{cl} = 0.096$, which is significantly lower than the currently used $a_{cl} = 0.144$.

To examine the sensitivity of a fog layer to τ_{cl}, the evolution of the fog layer was investigated by running the model with reduced values of τ_{cl}. As τ_{cl} depends linearly on both γ and a_{cl}, a reduction in either of them is equal to a percent-wise reduction of a_{cl}. Performed experiments include a lowering of a_{cl} to 0.096 (inducing a reduction in τ_{cl} to 67% of its original value), an experiment in which both a_{cl} and γ are reduced to 0.096 and 0.7 respectively (inducing a reduction in τ_{cl} of 47% of its original value) and experiments in which τ_{cl} is reduced to 25% and 10% of its original value. A lowering of a_{cl} to 0.096 induces a reduction in τ_{cl} of 67%, which is very close to the reduction induced by reduction of γ to its original value 0.7 (70%). Their impact can therefore can not be investigated separately.

The evolution of fog thickness and fog height in the Musc experiments with lowered values of τ_{cl} are presented and compared to the reference experiments in figure 9.3C-J. As expected, lowering τ_{cl} limits both the vertical growth and the cloud water content of the fog. For all experiments with lowered τ_{cl} cloud droplets are formed in L1 prior to fog initialisation in L0. This reveals that L0 is more sensitive to the feedback mechanism in which longwave emission by cloud water droplets enhances the cooling of a model layer, thereby accelerating fog formation. When this mechanism is weaker due to a lowering in τ_{cl}, fog formation in L0 is delayed. L0 consequently cools less strongly with increasing cloud water content (figure 9.5), as it receives a downward longwave flux from the overlying layer from the beginning onward. By comparison of the temperature decrease in L0 in the reference experiments to the experiments with lowered τ_{cl}, the contribution of cloud water to the cooling of L0 is clearly visible in figure 9.6K,L. While L0 cools steadily by -0.6 $\frac{K}{hr}$ in the experiments with lowered τ_{cl} where no fog is present yet, the cooling rate increases to -2.2 $\frac{K}{hr}$ when cloud water forms shortly after midnight in the reference experiment.

Although cloud water content in L1 increases less with decreasing τ_{cl}, the timing of fog initialisation in this layer is less sensitive to τ_{cl}. This is a result of the fact that the longwave cooling of a layer is

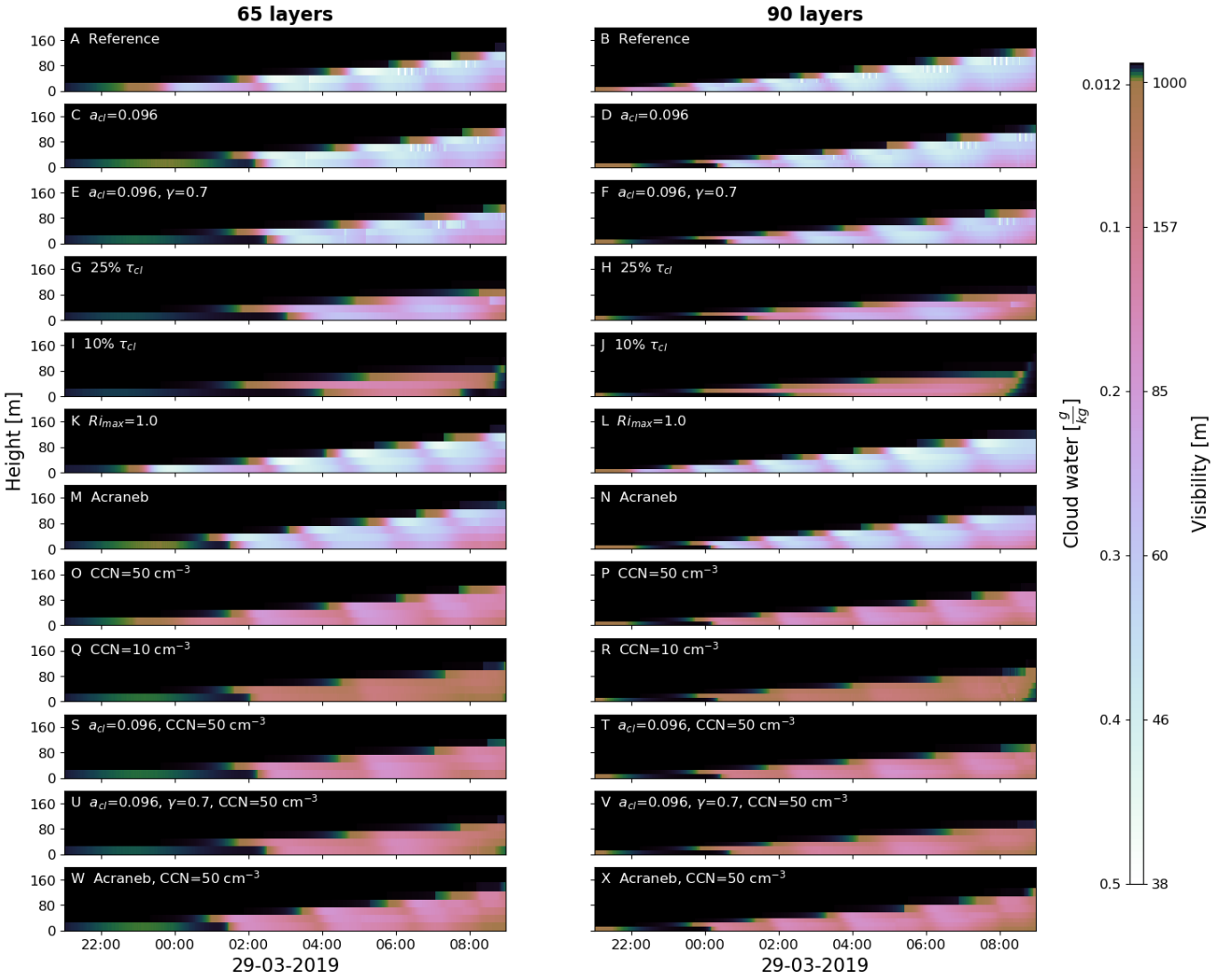

Figure 9.3: *Cloud water forecasts by Musc using a vertical resolution of 65 layers (left column) and 90 layers (right column) from various tests with Musc. In the different subplots the changed settings with respect to the reference experiments (A, B) are described.*

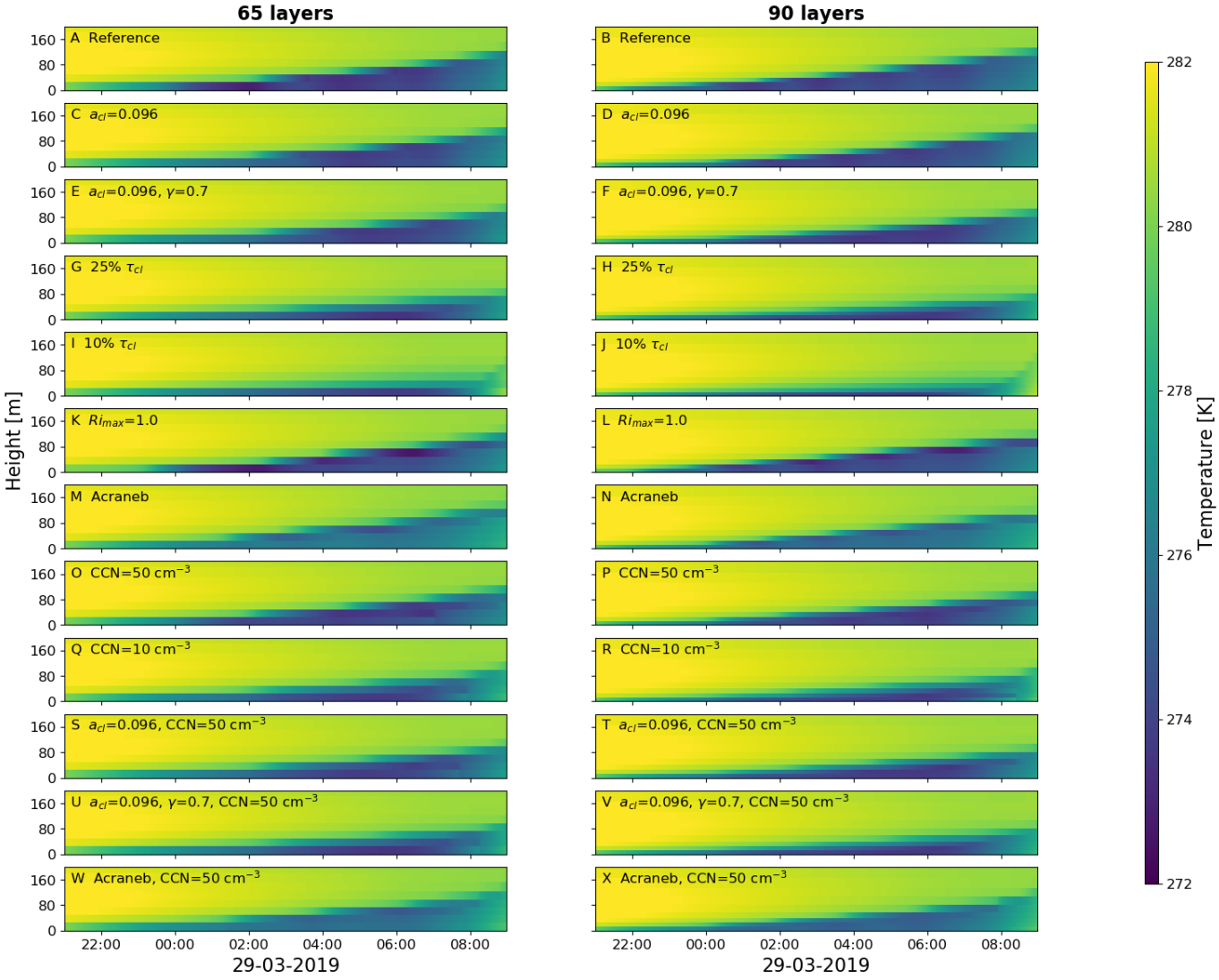

Figure 9.4: *Temperature forecasts by Musc using a vertical resolution of 65 layers (left column) and 90 layers (right column) from various tests with Musc. In the different subplots the changed settings with respect to the reference experiments (A, B) are described.*

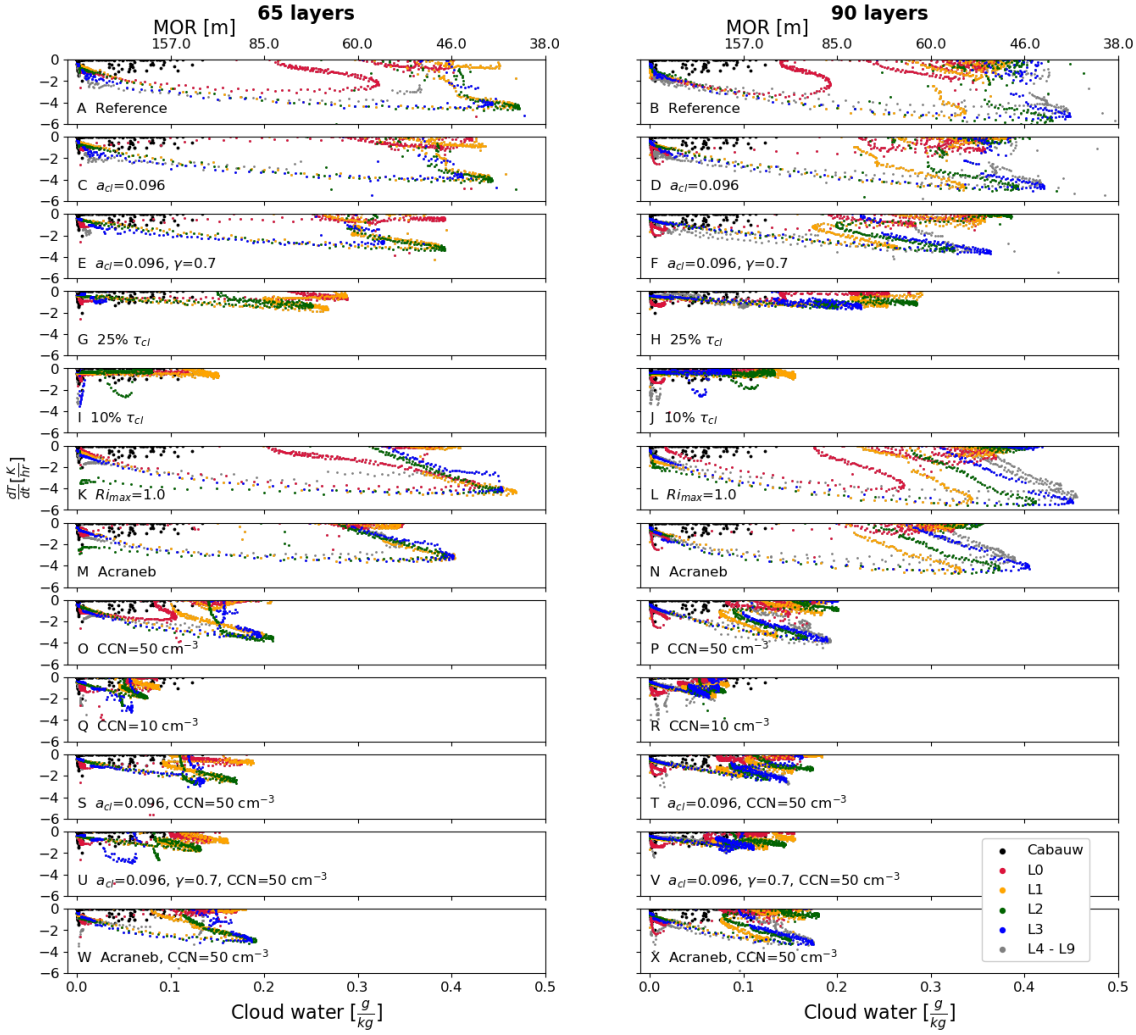

Figure 9.5: *Temperature change over time against cloud water content from various tests with Musc. In the different subplots the changed settings with respect to the reference experiments (A, B) are described. Cabauw observations during the fog case of 28/29 March 2019 are plotted in each figure for comparison. The upper x-axis indicates the MOR that corresponds to a cloud water content following equation 5.12.*

much more sensitive to cloud water content in the layer when the LWP is smaller than the blackbody depth. As visible in figure 9.2, this blackbody depth is about 40 $\frac{g}{m^2}$ for the reference experiments. While the LWP is 7.4 $\frac{g}{m^2}$ at 00:00 in Ref-65L, this LWP increases to 20.2 $\frac{g}{m^2}$ at 03:00 A.M when fog forms in L1. A decrease in τ_{cl} raises the blackbody depth of the fog, which decelerates fog formation in L0 but not in higher layers as the LWP rises too fast during their formation stage. Moreover, the independent behavior between L0 and L1 indicates that turbulent exchange has minor influence in the experiments.

The cooling rate per cloud water content in L1 and higher layers is strongly dependent on τ_{cl} (figure 9.5). While a fog layer of 0.1 $\frac{g}{kg}$ in REF-65L cools by 2.8 $\frac{K}{hr}$, the cooling rate decreases to 2.3, 1.9, 0.9 and 0.4 $\frac{K}{hr}$ for reduced values of τ_{cl} to 67%, 47%, 25% and 10% respectively. The maximum cooling rate measured at Cabauw during the fog case study of 28/29 March was 1.0 $\frac{K}{hr}$ for a 0.1 $\frac{g}{kg}$ fog layer, which corresponds to reported values for longwave radiative cooling rates measured in natural fogs with a similar cloud water density (Wærsted et al. 2017). A reduction of τ_{cl} to 25% closely fits these observations, confirming that a reduction of τ_{cl} in Harmonie potentially contributes to a more realistic representation of the longwave emissivity of fog.

These experiments only involve one single aspect of the problems with fog simulation in Harmonie and show that an adjustment within the physical boundaries does improve the model, but not fully solve the problem. The results of this method thus only indicate a single source of error but do not yet provide a key to a solution of the problem, for it can not be guaranteed that the overestimated fog layer growth in Harmonie is exclusively caused by the large τ_{cl}. However, the results demonstrate to what extend the reduction of τ_{cl} reduces the growth rate of a fog layer. The forecasted fog resembles the Cabauw observations of 28/29 March 2019 best when τ_{cl} is reduced to 10-25% of its original value, both in cloud water content as well as temperature and radiation budget. Such a large adjustment of τ_{cl} is however physically unjustifiable, which underlines that viewing the problem through a microscope must be avoided. However, as strong indications exist that the current parametrization of ϵ is no longer up-to-date, a lowering of τ_{cl} to 67% (by lowering a_{cl} to 0.096) is a suggested improvement to the longwave radiation scheme. The applicability of this new parametrization in Harmonie is tested in a 3D experiment in Chapter 10. Here, the three-dimensional impact of a lowering of τ_{cl} to 47% (by lowering a_{cl} to 0.096 and γ to 0.7) is evaluated as well. Although a small reduction can be justified,

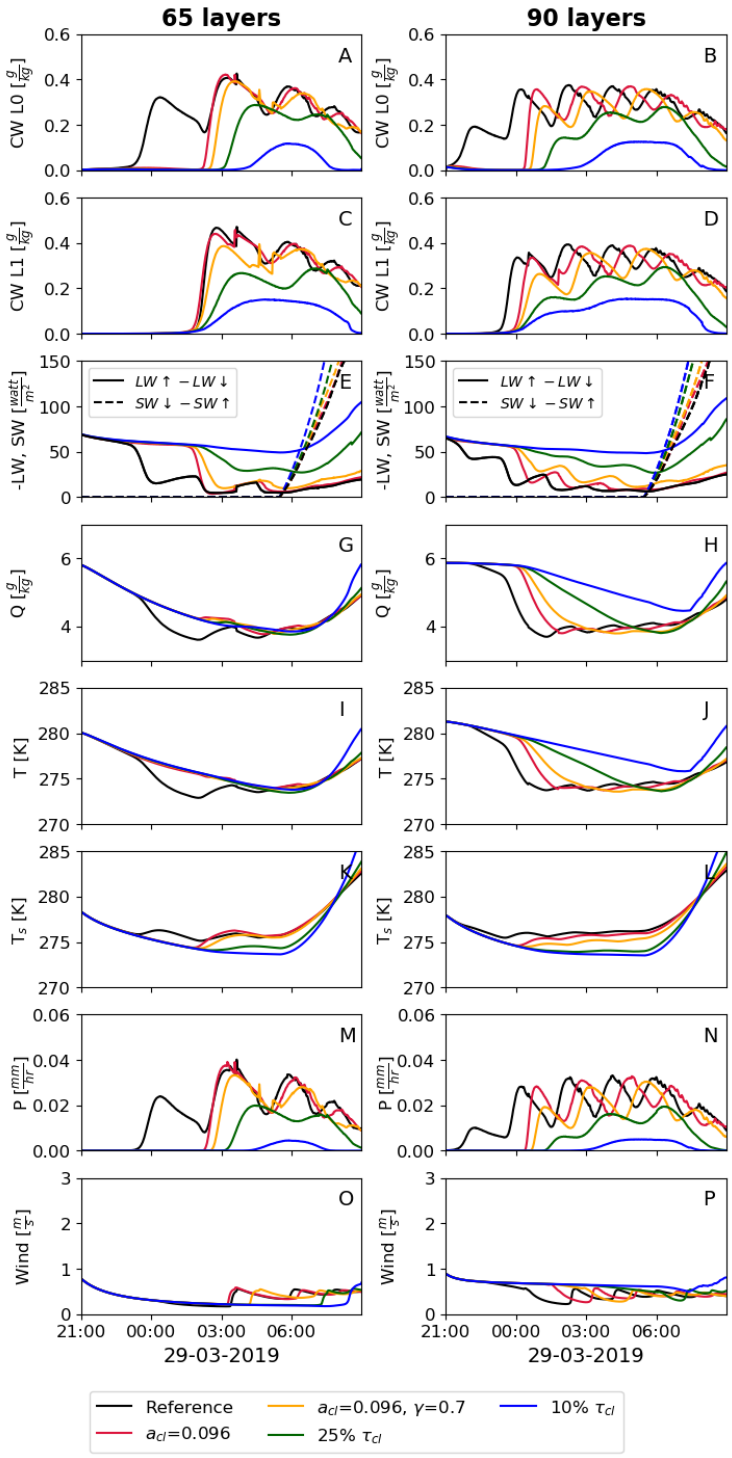

Figure 9.6:

Musc forecasts from various tests regarding reduced longwave emissivity values, with a vertical resolution of 65 layers (left column) and 90 layers (right column). Displayed tests differ from the reference experiment as indicated by their label. (A, B) Average cloud water in L0 (surface atmospheric layer, see table 5.1). (C, D) Average cloud water in L1. (E, F) Net outgoing longwave radiation and net incoming shortwave radiation at Earth's surface. (G, H) Average specific humidity in the lowest 23m-thick atmospheric layer. (I, J) Temperature in L0. (K, L) Surface temperature in L0. (M, N) Total precipitation at Earth's surface. (O, P) Average wind speed in L0.

the lowering of γ from 1.0 to 0.7 is a very debatable change. However, in its current form γ linearly reduces the longwave emissivity and as inclusion of γ=0.7 improves the correlation between temperature decrease and fog growth it is interesting to see the impact of a lowered longwave emissivity to 47% on fog evolution in Harmonie.

9.3 Testing the maximum Richardson number

The maximum Richardson number Ri_{max} is used to compute the exchange of energy and water between the surface and the lowest model layer. In this section, the impact of Ri_{max} on the evolution of fog is tested to examine whether the limitation of Ri_{max} to 0.0 is still valid since CANOPY was turned off in the SURFEX scheme (section 5.3.5). Two alternative settings of Ri_{max} were therefore tested; Ri_{max}=0.2 which was the case before 2012, and Ri_{max}=1.0 which practically means that the Richardson number is not limited. As both settings showed the same results (Ri did not exceed 0.2) only the results of Ri_{max}=1.0 are shown.

In figure 9.3K,L the evolution of cloud water over time is displayed for this experiment under 65 and 90 layer resolution. While the cloud water content and vertical extent are roughly unaltered in the 65 layer experiment, the fog growth is slightly limited under increased vertical resolution. The fog in L0 grows thicker when Ri_{max} is increased, which is a result of the reduced dew deposition and consequently higher Q. Furthermore, the fast fluctuations in cloud water and precipitation disappear under increased Ri_{max}. These fluctuations seem therefore related to interactions between cloud water and the surface fluxes.

The reduced exchange of heat between Earth's surface and L0 under higher Ri_{max}=1.0 results in a faster drop of T_s during the first hours of the run while L0 is less cooled from below. This effect is more pronounced under a 65 layer resolution than under a 90 layer resolution. However, the timing of the supersaturation in L0 is roughly similar to the timing in the reference experiments, which is a consequence of the higher Q.

To conclude, the main differences imposed on fog formation when Ri_{max} is increased, are observed in

the very initial stage when the reduced exchange of heat and humidity between the surface and L0 affect the initialisation of fog. After the formation of this layer, the consequences to the further evolution of the fog are limited.

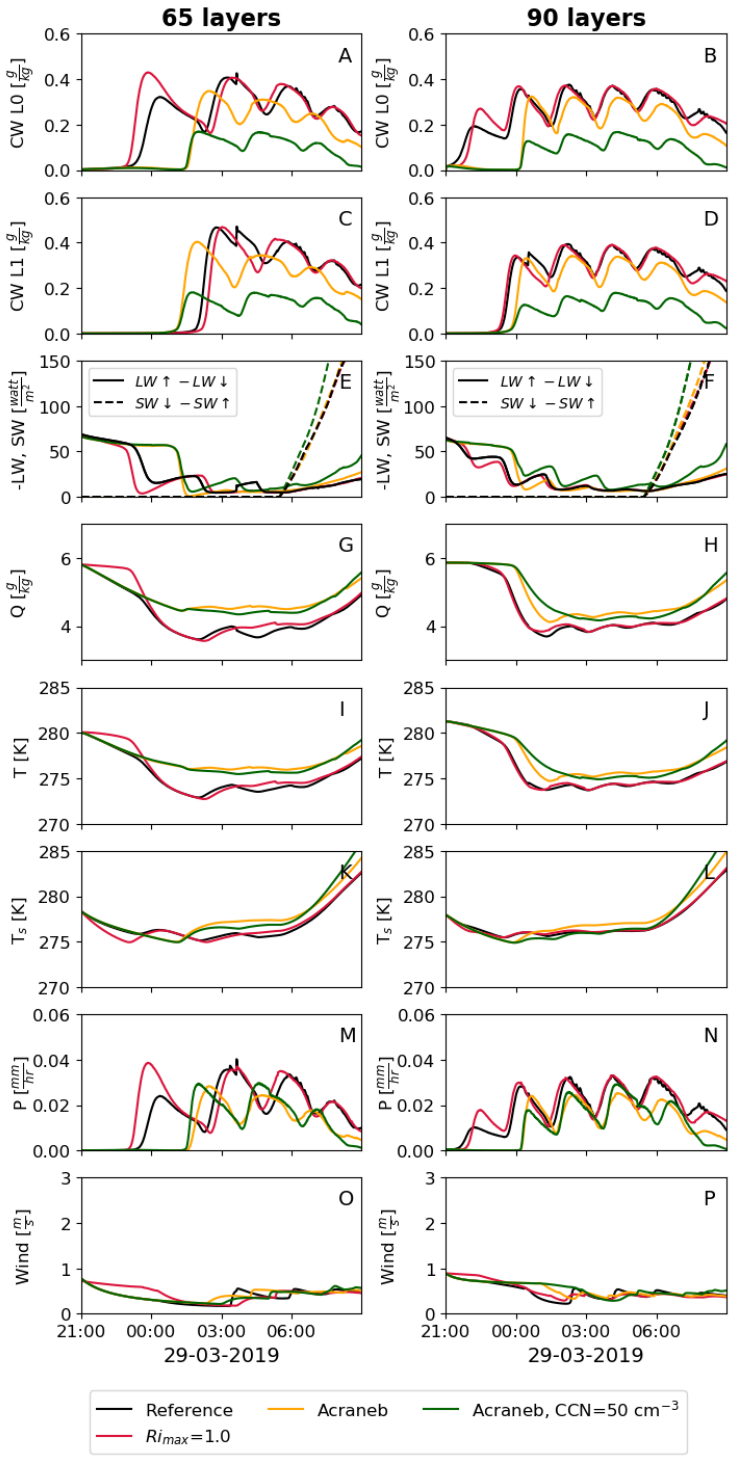

Figure 9.7:

Musc forecasts from various tests, with a vertical resolution of 65 layers (left column) and 90 layers (right column). Displayed tests differ from the reference experiment as indicated by their label. (A, B) Average cloud water in L0 (surface atmospheric layer, see table 5.1). (C, D) Average cloud water in L1. (E, F) Net outgoing longwave radiation and net incoming shortwave radiation at Earth's surface. (G, H) Average specific humidity in the lowest 23m-thick atmospheric layer. (I, J) Temperature in L0. (K, L) Surface temperature in L0. (M, N) Total precipitation at Earth's surface. (O, P) Average wind speed in L0.

9.4 Testing the radiative transfer scheme ACRANEB

The identification and adjustment of systematic errors of the interaction between fog and longwave radiation in RRTM is a major objective in this thesis. Besides comparison of the model results to observations, model results are also compared to model runs using an independent external radiation scheme. The radiative transfer scheme that is used for reflection is the single spectral interval scheme ACRANEB v.2 (Mašek et al. 2016; Geleyn et al. 2017, hereafter referred to as Acraneb), which has been used in the ALADIN NWP model since 1990 (Termonia et al. 2018). As Acraneb was developed independently from IFSRADIA, possible differences in the longwave radiation budget and the impact of fog may help to identify possible systematic errors in RRTM. In contrast to IFSRADIA (section 5.3.1), Acraneb is a broadband scheme using a single spectral band for shortwave radiation, and one for longwave radiation. Optical properties of water droplets, atmospheric gases and aerosol particles are derived from the same input as in IFSRADIA. Full cloud-radiation computations are performed at each timestep.

The goal is to identify and understand the dissimilarities between RRTM and Acraneb by intercomparison of model results with a similar setup. In this way, the impact of adjustments to radiation parametrizations in RRTM is reflected in the light of an independent external radiation scheme in an equal framework. In this section, the results of a Musc experiment using the radiative transfer scheme Acraneb are examined to obtain further insight in the possible systematic errors in the default longwave radiation scheme RRTM in Harmonie.

The cloud water forecasts from the experiments with Acraneb are less dense, which is most pronounced in L0 (9.3M, N). The cloud water concentration does not reach a critical amount in the Acraneb experiment at which the fog growth is enhanced by longwave cooling in the first model hours. From 21:00 A.M. to 23:00 A.M., cloud water in both Ref-65L and Acraneb with 65 levels (Acraneb-65L) rise to 0.012 $\frac{g}{kg}$. While the fog growth in the reference experiments is enhanced by longwave cooling, the cloud water content in Acraneb-65L falls back to zero until the layer is sufficiently cooled from the surface.

In Acraneb-65L, the fog initializes in L1 one hour earlier than in Ref-65L, and consequently grows higher. However, in the 90 layer experiment the timing of fog initialisation in L1 and higher layers is similar to Ref-90L. The timing difference under 65 layers may be a consequence of the reduced cooling in L0 (figure 9.4M, N), leading to less stability and more vertical mixing. This has a larger impact under 65 layers, as L0 is thicker in this experiment. Maximum cloud water concentrations are 0.06 $\frac{g}{kg}$ (65 layers) and 0.05 $\frac{g}{kg}$ (90 layers) lower than in Ref-65L and Ref-90L.

The temperature drop in the fog layers is in all layers less pronounced in the Acraneb experiments (figure 9.4M, N), which results in L0 in a difference up to 5.2K between Acraneb (65 layers) and Ref-65L. Figure 9.5M, N shows that this is not only a consequence of the lower cloud water content as well as the lower emissivity of the fog. Although the temperature drop per cloud water content is equal to the reference experiments for light fog, the correlation curve between temperature decrease and cloud water content flattens more with increasing cloud water content than in the reference experiments.

The positive feedback between cloud water and temperature decrease is less pronounced when using Acraneb. This supports the hypothesis that this feedback mechanism in RRTM is too strong, as results from the experiments with Acraneb resemble the results from experiments with RRTM using a reduced τ_{cl} to 50-70%. Furthermore, the fast oscillations in temperature and precipitations do not occur in Acraneb, which therefore origin in the interaction between cloud water and radiation in RRTM.

9.5 Testing the amount of cloud condensation nuclei

A very interesting and relevant point was brought up by Yann Seity (Météo-France, personal communication) regarding the influence of the microphysical scheme on radiative cooling. Fog forecasts from AROME-France show similar problems as observed in Harmonie; after initialisation of fog in a layer, this layer starts to cool too strongly (up to 6 $\frac{K}{hr}$ as well) and the fog layer grows too fast and dense. Interestingly, AROME-France is also run in parallel with the microphysical scheme LIMA instead of ICE3. In parallel runs with LIMA, the radiative cooling is strongly reduced to a maximum of 3.3 $\frac{K}{hr}$. The cooling is furthermore not isolately observed in the upper fog layer, but spread over a deeper layer (50-60 m) as also the two underlying layers are cooling at a similar rate as the highest layer. Furthermore, the cloud

water content in fog is lower under LIMA. While the maximum cloud water content in fog during an AROME-France run with ICE3 was between 0.3 and 0.4 $\frac{g}{kg}$, this was reduced to about 0.15 $\frac{K}{hr}$ (and quickly decreased to 0.1 $\frac{K}{hr}$ after its maximum) when LIMA was used as the microphysical scheme. The total amount of cloud water is thus smaller when using LIMA, and subsequently the impact of the fog on longwave radiation is smaller.

The difference between LIMA and ICE3 may originate from an extra parameter that is included in LIMA, which describes the droplet number concentration in addition to the mixing ratio. The inclusion of this parameter enables a more sophisticated description of the microphysical properties over time. While both the droplet number concentration and liquid water content are high during the initial phase of fog formation, both decrease with time. Consequently, the maximum amount of water droplets (which is 300 cm^{-3} in AROME-France) is only reached shortly, after which it decreases to about 100 cm^{-3} after one hour, and to less than 50 cm^{-3} after two hours. A side-effect of the growth of fog droplets is stronger settling, resulting in reduced cloud water content in the fog. In contrast, the droplet number concentration in ICE3 follows from the prescribed CCN, which is 300 cm^{-3} for continental air masses and 100 cm^{-3} for maritime air masses. With ICE3, the droplet number concentration is consequently constant over time, and thereby higher than with LIMA. Moreover, droplet number concentrations in LIMA are closer to observed values, as Mazoyer et al. (2019) measured droplet number concentrations of 49-98 cm^{-3} for thick radiation fog layers (section 4.1).

In this section, the prescribed values for CCN are reduced to test their impact on fog evolution. A reduced amount of CCNs can affect fog by limiting the amount of water droplets that form and reducing its lifetime by a faster precipitation release (section 4.1). The prescribed values were previously set to 300 cm^{-3} for continental air masses and 100 cm^{-3} for maritime air masses. Both values are set to 50 cm^{-3}, 25 cm^{-3} and 10 cm^{-3} in the performed Musc tests described in this section. Besides the tests with reduced CCN and with other settings equal to the reference experiments, three other simulations are performed under reduced CCN to 50 cm^{-3}; a simulation with CCN=50 cm^{-3} and reduced a_{cl} to 0.096, and a simulation with CCN=50 cm^{-3}, reduced a_{cl} to 0.096 and reduced γ to 0.7 and a simulation with CCN=50 cm^{-3} and Acraneb.

The impact of reduced CCN on the evolution of cloud water is displayed in figure 9.3O-W. The cloud water concentration in the fog is strongly lowered. With CCN=50 cm^{-3}, the cloud water content is limited to a maximum value of 0.22 $\frac{g}{kg}$ (65 layers) and 0.20 $\frac{g}{kg}$ (90 layers). When CCN is further reduced to 10 cm^{-3}, the cloud water content is further limited to 0.08 $\frac{g}{kg}$ for both vertical resolutions. The CCN concentration only little affects the timing of initialisation and the vertical expansion of the fog. Furthermore, the cooling of the layer is reduced as a consequence of the lower cloud water concentration, but the maximum cooling rate per cloud water content is not affected (figure 9.5). A small increase with decreasing CCN could be expected here from the definition of τ_{cl}, which depends as $\tau_{cl} \sim \text{CCN}^{-\frac{1}{3}}$ for a given liquid water path (equation 5.2-5.4). The impact of the increased τ_{cl} on the longwave cooling in the fog is counteracted by the decreased LWC in the underlying layers, which are consequently less cold compared to the reference experiments (figure 9.8I, J). The loss of heat towards these layers is smaller, which is also visible in figure 9.8I, J by the decreased increase in temperature in L0 at 02:00 A.M., when fog enters L1. The amount of precipitation with CCN=50 cm^{-3} is reduced by only 6%, which is very little compared to the 50% reduction in cloud water content. As expected, the loss of water to precipitation is thus relatively large when CCN is decreased due to the larger cloud water droplets.

Combining a reduction of CCN to 50 cm^{-3} with a reduction in a_{cl} to 0.096 reduces the LWC further, reaching a maximum value of 0.19 $\frac{g}{kg}$ (65 layers) and 0.17 $\frac{g}{kg}$ (90 layers). The impact on the maximum cooling rate per cloud water content is similar to the original experiments with reduced a_{cl} to 0.096.

When the simulation with CCN=50 cm^{-3} and a_{cl}=0.096 is repeated including inhomogeinity factor γ=0.7 as well, the LWC is further reduced to the maximum value of 0.17 $\frac{g}{kg}$ (both 65 and 90 layers) and the vertical expansion of the fog is limited. For the experiment with 65 layers, maximum LWC amounts to 37% of its original value in Ref-65L. This is close to the desired reduction, as the LWC in fog measured at Cabauw during the case study of 28/29 March amounts to 44% of the overestimated Harmonie-65L simulation (section 8). The cooling rate per liquid water content is also close to the Cabauw observations (figure 9.5). However, the vertical expansion of the fog is only slightly reduced. The results from the simulation combining Acraneb and CCN=50 cm^{-3} result in fog behavior similar to the simulation with CCN=50 cm^{-3} and a_{cl}=0.096, which shows that for a given longwave emissivity changed fog behavior resulting from CCN reduction is not affected by the specific radiation scheme.

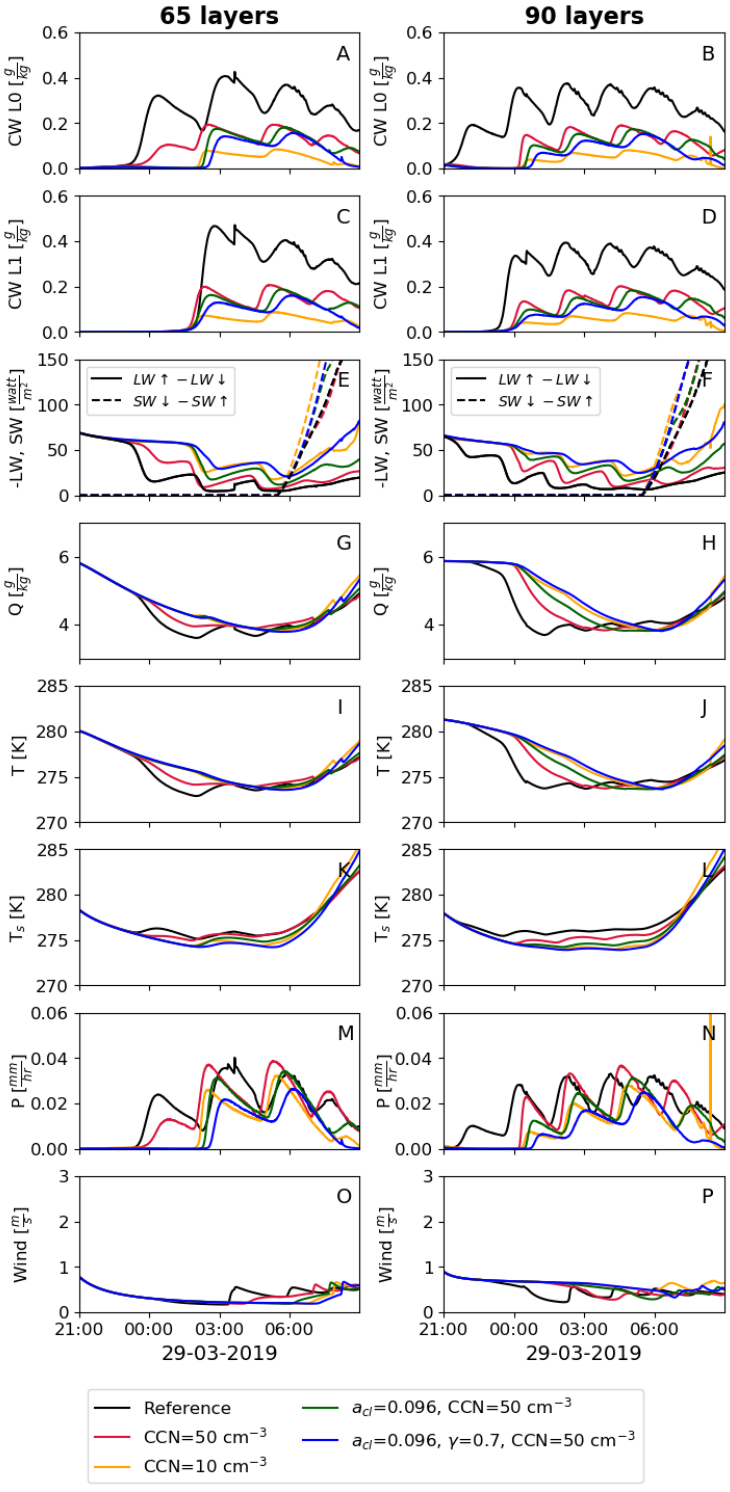

Figure 9.8:

Musc forecasts from various tests, with a vertical resolution of 65 layers (left column) and 90 layers (right column). Displayed tests differ from the reference experiment as indicated by their label. (A, B) Average cloud water in L0 (surface atmospheric layer, see table 5.1). (C, D) Average cloud water in L1. (E, F) Net outgoing longwave radiation and net incoming shortwave radiation at Earth's surface. (G, H) Average specific humidity in the lowest 23m-thick atmospheric layer. (I, J) Temperature in L0. (K, L) Surface temperature in L0. (M, N) Total precipitation at Earth's surface. (O, P) Average wind speed in L0.

9.6 Conclusions from Musc simulations

To conclude, the cooling rate per cloud water content is strongly dependent on τ_{cl}, and introduction of lower a_{cl}=0.096 and γ=0.7 reduces the cooling rate in a fog layer of 0.1 $\frac{g}{kg}$ from 2.8 to 1.9 $\frac{K}{hr}$, while the maximum cloud water content in the fog decreases to 0.38 $\frac{g}{kg}$. Simulations using the radiative transfer scheme Acraneb and increased Ri_{max}=1.0 resulted in limited changes. A reduction of CCN to 50 cm^{-3} reduces the maximum amount of cloud water from 0.46 to 0.22 $\frac{g}{kg}$ (65 layers), but does not affect the maximum cooling rate per cloud water content in the fog layers. The fog simulation in Musc resembles Cabauw observations most when the reduction of CCN to 50 cm^{-3} is combined with a reduction in a_{cl} and γ, as the amount of cloud water is then further limited to a maximum of 0.17 $\frac{g}{kg}$ and the maximum cooling rate is largely limited to less than 2.0 $\frac{K}{hr}$. Isolately lowering τ_{cl} to 25% or lowering CCN to 10 cm^{-3} leads to similar cloud water contents but these adaptations are physically unjustifiable.

However, the fast vertical expansion of the fog is still an issue, as no experiments (with exception of reducing τ_{cl} to unrealistic low values) did strongly limit this. Furthermore, the fog in the Musc reference experiments also developed thicker than in the simulations with Harmonie. This might be a problem related to the usage of Musc, as weak advection is present in Harmonie, but not in Musc. As a fog layer is colder than its environment, the horizontal outflow of fog can lead to weak descendance of the air, thereby limiting the vertical growth. This effect is not present in Musc, and a larger vertical impact may appear in the 3D Harmonie tests. A best combination of the adaptations in a_{cl}, γ and CCN is therefore further explored in Harmonie Cy43h2.1 (target 1).

10 Testing with Harmonie

Based on the results of the performed Musc experiments, three experiment setups were selected to test in 3D Harmonie experiments. While Harmonie Cy40h1.1.1 is currently operationally run at KNMI, the target model cycle is Harmonie Cy43h2.1 (target 1) as KNMI will switch to this cycle in the future. The experiments are therefore run with Harmonie Cy43, as well as a new reference experiment with 65 layers. No experiments with increased vertical resolution are included, as this did not improve the fog simulation in Harmonie Cy40h1.1.1 as well as the Musc experiments. Although consequences of increasing Ri_{max} were limited to the very initial state in Musc, a Harmonie Cy40 simulation with Ri_{max}=1.0 was previously run by Sander Tijm at KNMI and showed to have considerable impact on the fog evolution. This experiment is consequently presented here as well, to give a complete overview of model adjustments that are currently under research. The included Harmonie experiments are the following:

1. A reference Harmonie Cy40 experiment (H40 Ref-65L).
2. A Harmonie Cy40 experiment using Ri_{max}=1.0.
3. A reference Harmonie Cy43 experiment (H43 Ref-65L).
4. A Harmonie Cy43 experiment with lowered a_{cl}=0.096.
5. A Harmonie Cy43 experiment with lowered a_{cl}=0.096 and lowered γ=0.7.
6. A Harmonie Cy43 experiment with lowered a_{cl}=0.096 and lowered CCN=50 cm^{-3}.
7. A Harmonie Cy43 experiment with lowered a_{cl}=0.096 and lowered CCN=25 cm^{-3}.
8. A Harmonie Cy43 experiment with lowered a_{cl}=0.096, lowered γ=0.7 and lowered CCN=50 cm^{-3}.
9. A Harmonie Cy43 experiment with lowered a_{cl}=0.096, lowered γ=0.7 and lowered CCN=10 cm^{-3}.

The results of these experiments are shown and discussed in this section. All model runs start at 28 March 2019 12:00 UTC for a model resolution of 65 layers. Apart from the location of the Cabauw

observatory, the consequences of the adjusted parametrizations on the evolution of fog over a location in the North Sea (51°59'42.90"N, 3°40'02.80"E) is evaluated as well.

10.1 Comparing Harmonie Cy43 to Harmonie Cy40

When the simulation of the case study of 28/29 March 2019 is repeated with Harmonie Cy43, a fog layer develops which is already less dense, deep and extensive compared to the fog layer simulated with Harmonie Cy40. The differences between both Harmonie versions are described in section 7.4. Unexpectedly, the fog behaves very differently in Harmonie Cy43. The fog grows too thick and expands too much in horizontal and vertical extent compared to Cabauw observations, but to a much lesser degree than in Harmonie Cy40. The difference between figure 10.1A and C shows that the fog expansion over land is strongly reduced in Harmonie Cy43, while differences over sea are smaller. The vertical growth at Cabauw is limited to 47 m with Harmonie Cy43, reaching a maximum cloud water content of 0.22 $\frac{g}{kg}$, which is still higher than the maximum cloud water content deduced from visibility measurements at Cabauw (0.16 $\frac{g}{kg}$) but to a lesser degree than forecasted using Harmonie Cy40 (0.36 $\frac{g}{kg}$) (Chapter 8).

Which revisions in Harmonie Cy43 may have contributed to the reduced fog expansion compared to Harmonie Cy40? Experiments from Emily Gleeson (Met Éireann, Ireland, personal communication) point out that the fog is very sensitive to settings in the surface roughness. As there are large differences in roughness between Cy40 and Cy43, this probably causes the diminished fog expansion in Cy43. Furthermore, the impact of the novel option to include height dependence of aerosols in Harmonie Cy43 may already lead to a decline in CCN on the lowest model level, thereby reducing fog density. However, this impact is very small, especially compared to the impact of reducing CCN to 50 cm^{-3} as described in section 10.3. The reason for the different fog behavior between Cy40 and Cy43 is still under research.

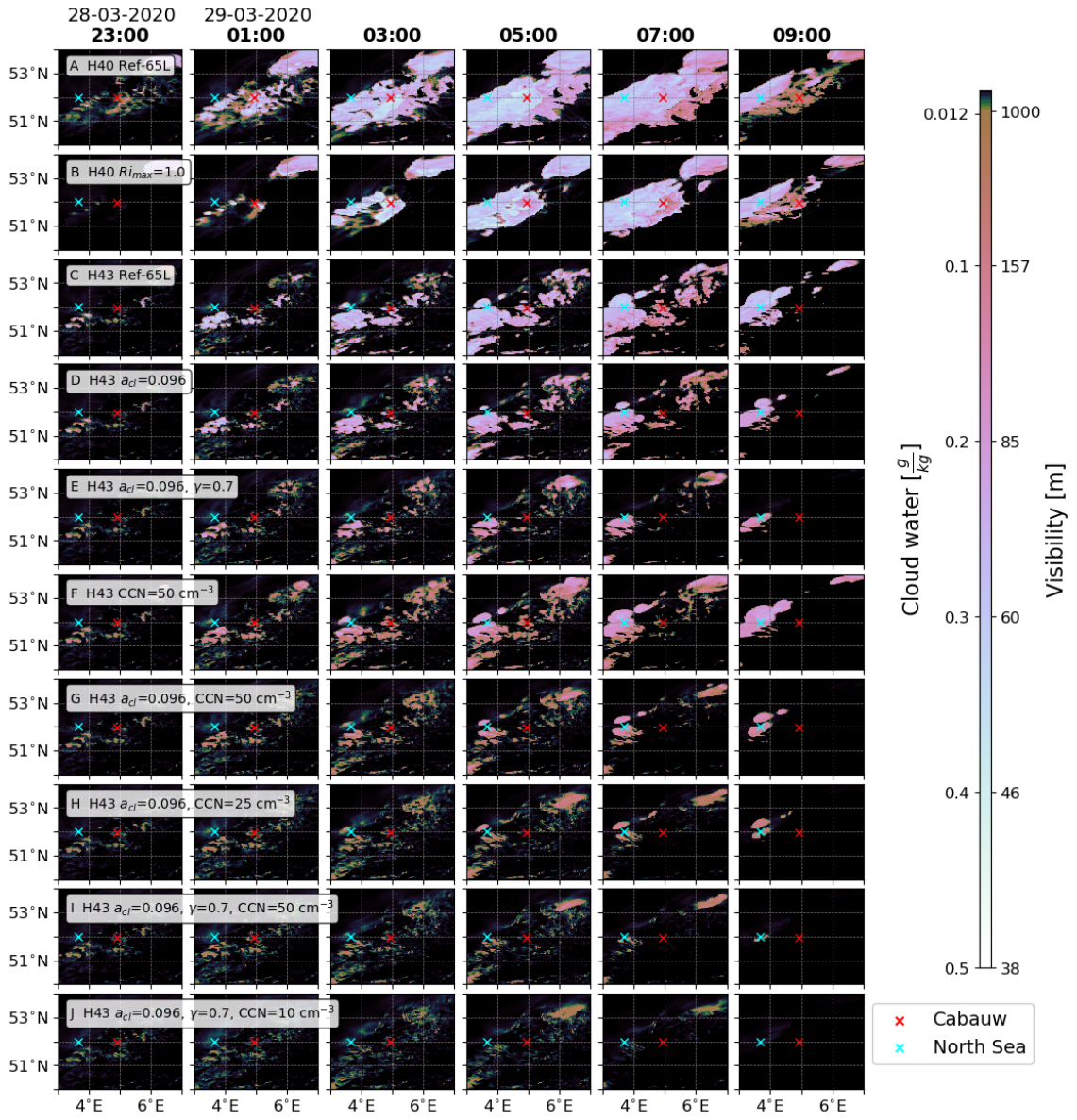

Figure 10.1: *Cloud water forecasts of various Harmonie experiments at vertical level L0. Timesteps are indicated above each column. H40 Refers to experiments performed with Cy40h1.1.1, H43 refers to experiments with Harmonie Cy43h2.1 (target 1). In the different subplots the changed settings with respect to the reference experiments (A for H40, C for H43) are described.*

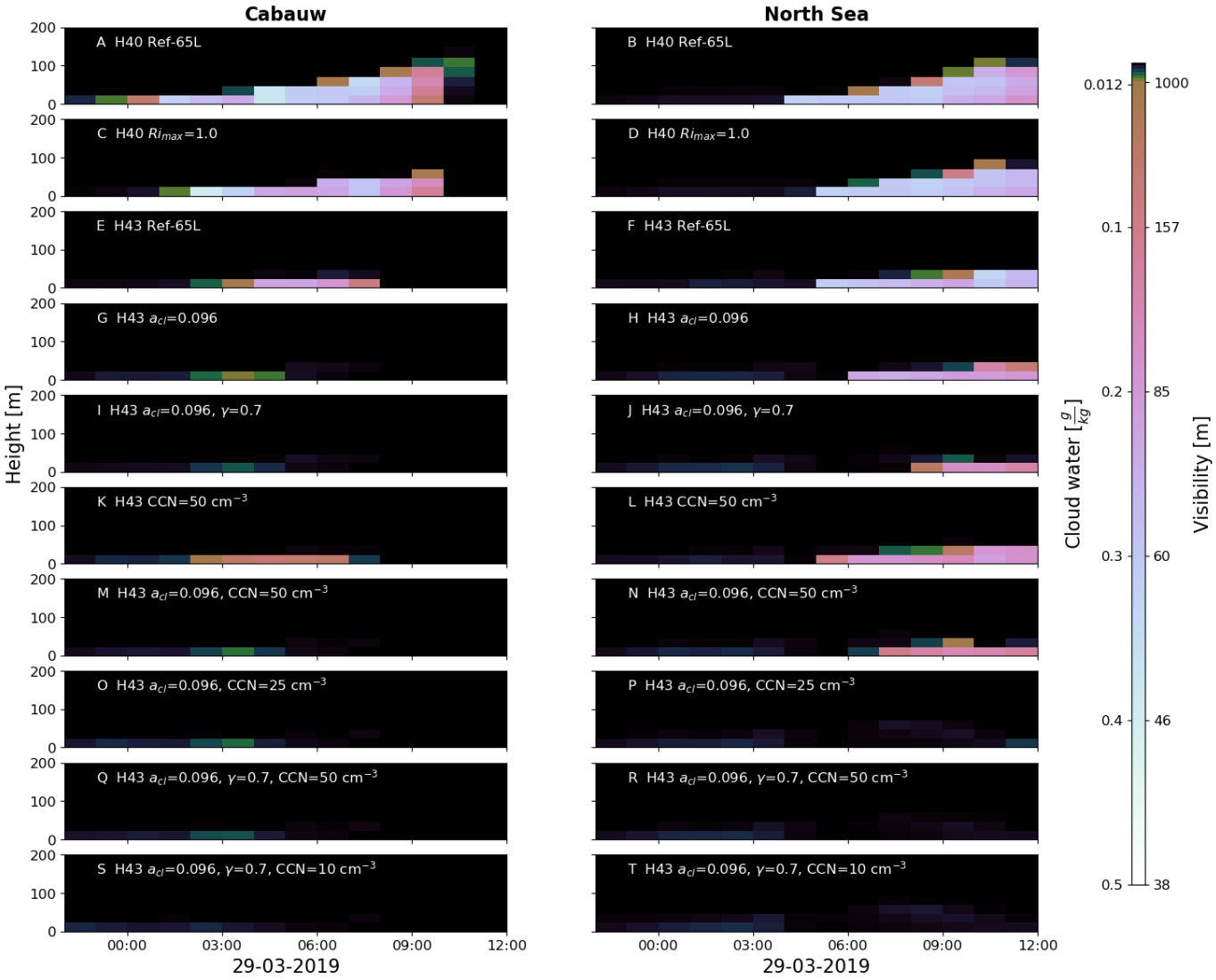

Figure 10.2: *Cloud water forecasts by Harmonie using a vertical resolution of 65 layers at Cabauw (left column) and over the North Sea (right column, location indicated in figure 10.1) from various tests. H40 Refers to experiments performed with Cy40h1.1.1, H43 refers to experiments with Harmonie Cy43h2.1 (target 1). In the different subplots the changed settings with respect to the reference experiments (A, B for H40, E,F for H43) are described.*

10.2 Testing the maximum Richardson number

Although consequences of increasing Ri_{max} were limited to the very initial state in the Musc experiment (section 9.3), the fog growth in Harmonie Cy40 (H40) is considerably reduced when Ri_{max} is increased from 0.0 to 1.0. Figure 10.1B shows how fog is initialised later over land, while fog formation over sea has little changed. The total land area covered by fog at 07:00 A.M. has declined by about 40% in comparison to the H40-Ref, while there is still as much fog over sea. This difference in impact on land and sea is to a lesser extent visible from the vertical cross sections of cloud water content in the fog (figure 10.2C, D). At both locations, the fog has reduced in both vertical extent by one model layer, but not in cloud water density under increased Ri_{max}.

From figure 10.3D is visible that the temperature in L0 using Ri_{max}=1.0 is 1.5 K higher than in H40 Ref-65L, showing that the reduction of turbulent surface fluxes leads to less longwave radiative cooling under clear skies. The fog initialised consequently later, causing the fog layer to have less time to expand before it is dissipated by radiative warming after sunrise. However, while the temperature in L0 and specific humidity decrease after sunset are underestimated in H40 Ref-65L, they are overestimated using Ri_{max}=1.0. The specific humidity before fog initialisation is 0.3 $\frac{g}{kg}$ higher than observed at Cabauw, in contrast to the 0.3 $\frac{g}{kg}$ underestimation in H40 Ref-65L. The overestimation of temperature and specific humidity indicate that the turbulent surface fluxes thus turn too small under Ri_{max}=1.0. Longer and more experiments are required to test its general impact.

10.3 Testing reduced longwave emissivity and cloud condensation nuclei

Many experiments are performed with Harmonie Cy43 (H43) to test the impact of different combinations in which a_{cl}, γ and CCN are reduced to differing degrees. Figure 10.1D-J shows the resulting horizontal cloud water distribution of the different experiments, that are indicated by their change with respect to H43 Ref-65L in which the original settings are used (a_{cl}=0.144, γ=1.0 and CCN=300 cm^{-3} over land

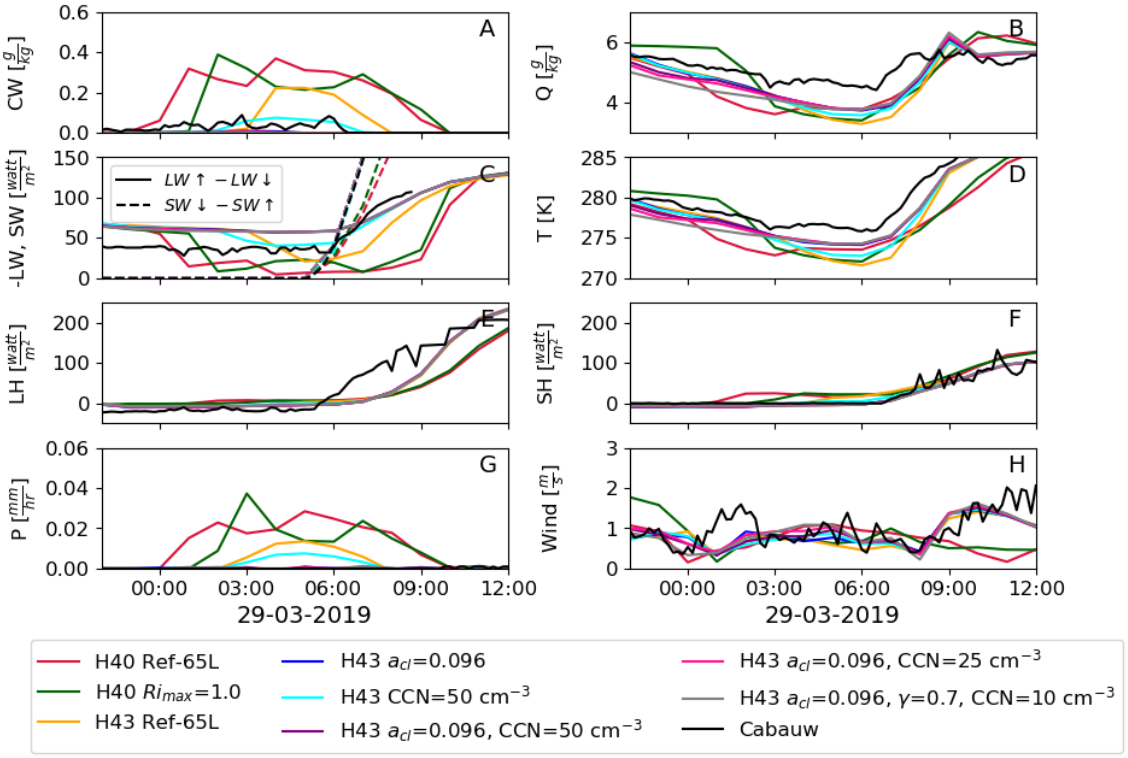

Figure 10.3: *Harmonie Cy43 forecasts from a selection of the experiments and Cabauw observations during 28/29 March 2019. In the experiment names define the changed settings with respect to Ref-H43-65L. (A) Average cloud water in the lowest 23m-thick atmospheric layer L0 (note: observed cloud water was deduced from Cabauw MOR observations). (B) Average specific humidity in the lowest 23m-thick atmospheric layer. (C) Net outgoing longwave radiation and net incoming shortwave radiation at Earth's surface. (D) Temperature in L0. (E) Latent heat flux at Earth's surface, positive when heat is transported away from the surface. (F) Sensible heat flux at Earth's surface, positive when heat is transported away from the surface. (G) Total precipitation at Earth's surface. (H) Average wind speed in L0.*

and 100 cm^{-3} over sea). In figure 10.2G-T vertical sections of the same experiments at Cabauw and the North Sea (as indicated in figure 10.1) are shown.

At Cabauw fog growth is limited to L0 in all experiments. With exception of H43 CCN=50 cm^{-3}, the cloud water concentration is underestimated here and the fog directly dissipates after sunrise. Over the North Sea, the impact of reducing CCN is smaller than over land, which can simply be explained by the fact that CCN is lower over sea than over land in H43 Ref-65L. Fog expansion over sea is overestimated in all experiments, with exception of H43 a_{cl}=0.096, γ=0.7 and CCN=50 cm^{-3}/10 cm^{-3}.

The evolution of different meteorological variables over time for a selection of the experiments is shown in figure 10.3. The net longwave radiation budget is much less affected by the fog in the experiments than in H43 Ref-65L, thereby better resembling the shape of the measured longwave radiation budget. However, the difference between the net longwave radiation under clear sky (70 $\frac{Watt}{m^2}$ in the experiments, 40 $\frac{Watt}{m^2}$ at Cabauw) shows a model aspect that could be interesting to investigate further. The temperature and specific humidity are underestimated for all tests, which before the fog initialisation correlates to the higher radiative heat loss. Until fog initialisation in L0 (about 03:00 A.M.) this underestimation is strongest for the most extreme experiments (H43 a_{cl}=0.096, γ=0.7 and CCN=50 cm^{-3}/10 cm^{-3}). This possibly is a consequence of the absence of higher clouds in the early night in these runs, and this may hint that the changes in CCN and emissivity lead to an underestimation of high clouds here. After fog initialisation, all experiments except CCN=50 cm^{-3} show a similar gradual cooling in contrast to the sharp drop in temperature with H43 Ref-65L, thereby showing the lower impact of cloud water on the temperature. With the reduction in liquid cloud water, the precipitation that was present in the reference experiments but not observed at Cabauw is dispensed.

11 Discussion

So far, only the impact of changed parametrizations on fog simulation in one specific setting has been discussed, and the question remains how changes in emissivity and CCN perform under other weather scenarios, including similar settings such as the development of radiation fog in other seasons, as well as totally different weather types. A wider view on the consequences of the proposed changes is required to ascertain their overall impact on the performance of Harmonie. There are many possible adaptations that may limit fog expansion and longwave radiative cooling, and profound reasoning based on the physics is required such that adaptations that do not only limit fog growth, but also bring the model calculations closer to meteorological processes in reality.

From a physical point of view, increasing spatial resolution is always an improvement. In the Musc tests that were performed with increased vertical resolution from 65 to 90 layers, fog grew mostly thicker and higher. This was a consequence of the cooling effect of the cloud droplets on a layer, which was stronger under increased resolution. The worse performance under increased resolution shows that the current parametrizations of both ground and atmospheric processes are not adapted to smaller height scales, and therefore not accurate enough. To see the real impact of the usage of a higher vertical resolution in Harmonie, it is important to evaluate which model components should be adjusted to scale first.

The physical argumentation to reduce emissivity a_{cl} from 0.144 to 0.096 is strong; the former parametrization was introduced in 1978. Since the aerosol content has strongly decreased and this parametrization was never tested in our domain, revision is required. Measurements at Cabauw show clearly that 0.144 is an overestimation under foggy conditions. However, the observations of emissivity in nighttime fog events show significant scatter around the relation that was found, and it could be interesting to study the reason for this scatter. Supplementary experiments are required to investigate whether the proposed relation is also valid to describe the emissivity of other cloud types (and liquid precipitation) that are described by the same parametrization. Furthermore, the sensitivity of cloud

emissivity to the atmospheric composition is large, and one should be cautious when the same emissivity is applied in another domain. The question arises whether the longwave emissivity is sufficiently correct represented by a parametrisation that depends on the LWP and droplet radius exclusively. Usage of a monochromatic value for longwave emissivity neglects differences in spectral transmittance between different air masses, which is for example higher in dry clear sky than in moist clear sky. The inclusion of more parameters may improve the validness of a relation that describes fog emissivity. Furthermore, it could be interesting to experiment with other methods describing the longwave optical properties of clouds within RRTM, such as the method of Lindtner and Li (2000) which is used at the ECMWF, or the Savijärvi (1997) method. Both methods include 16 sets of coefficients to compute the mass extinction coefficients for each individual spectral band, thereby accounting for differences in spectral transmittances for different air masses.

The reduction of the inhomogeinity factor γ from 1.0 to 0.7 is a very debatable change. Although a small reduction can be justified, cloud experts at KNMI have advised to leave it as close to 1.0 as possible as factor 0.7 is too small for 2.5-km grid cells. However, in its current form γ linearly reduces the longwave emissivity. As inclusion of γ=0.7 improves the correlation between temperature decrease and fog growth in the experiments in this thesis, it could be interesting to investigate whether the magnitude of a_{cl} should be reduced below 0.096, as this has a similar effect as reducing γ.

Regarding CCN, the usage of a constant value over time requires a compromise; while larger values lead to a more realistic droplet size distribution in initial fog, longer persisting fog is better represented under lower CCN. However, the current values of 300 cm^{-3} over land and 100 cm^{-3} over sea appear too large in all situations. The physical meaning of CCN is however debatable in this context; Emily Gleeson (Met Éireann, Ireland, personal communication) showed that the usage of CCN=50 cm^{-3} resulted in more realistic fog representation than the usage of realtime CCN. The usage of CCN as a tuning parameter therefore means that it does not represent the actual amount of CCN, but the amount of CCN that leads to the right amount of cloud droplets in Harmonie. It can be interesting to see how fog is affected other changes that lead to a decreased amount of cloud droplets, for example increased gravitational cloud droplet settling as described by Bengtsson (2007). The effect of reduced CCN seems to result in a better representation of the cloud droplet distribution in longer existing fog, but the question remains

whether this change now is compensating for other parametrizations that can be improved as well. From AROME-France experiments with LIMA it turns out that the inclusion of cloud droplet evolution to the microphysical scheme brings cloud water concentrations back to observed values. LIMA can not be implemented in Harmonie Cy43, but in Harmonie Cy46 LIMA can be tested which could be very interesting. In a broader view, the consequences of a decrease in CCN is expected to diminish cloud cover as well, thereby affecting the radiation budget and many other weather aspects. Furthermore, using an equal CCN over land and sea is hypothesized to improve precipitation at the coast, as this is now underestimated as the increase in CCN for air travelling from sea to land leads to the redistribution over smaller cloud droplets. The overall impact is difficult to anticipate and all parametrizations must be extensively tested before they can be introduced in Harmonie Cy43 for operational usage.

12 Conclusions

This thesis describes the analysis of a case study of the performance of the operational high-resolution weather model Harmonie on fog simulation, as well as the impact of several adjusted parametrizations. The performance of Harmonie on simulating radiation fog is studied by comparing Harmonie and Musc simulations to Cabauw observations. By evaluating the representation of physical processes related to radiation fog formation in HARMONIE-AROME, acute issues that may lead to erroneous forecasting are addressed. The aim is to find and evaluate parametrization adjustments that imporve the physical correctness of the model, as well as the model performance on fog simulation. The main focus lies on the representation of fog in the longwave radiation scheme and its dependence on the amount of cloud condensation nuclei. From the experiments it appears that the overestimation of fog is correlated to too strong longwave cooling by the fog. Based on the outcomes of many MUSC experiments, adaptations based on cloud emissivity (0.096 instead of 0.144), longwave cloud inhomogeneity (0.7 instead of 1) and the number of cloud condensation nuclei (10-50 cm^{-3} instead of 300 cm^{-3} over land and 100 cm^{-3} over sea) are tested with Harmonie. Other evaluated experiments include an increased vertical resolution (90 model levels instead of 65) the usage of the longwave radiation scheme ACRANEB and an increase of the maximum Richardson number Ri_{max} (1.0 instead of 0.0). This section summarizes the main conclusions that can be drawn.

A first conclusion is that a vertical increased model resolution does not improve fog simulation in Harmonie, pointing out that the current parametrizations of both ground and atmospheric processes are not representative using a smaller height scale.

This study confirms that increasing Ri_{max} limits horizontal and vertical fog expansion, but does not reduce the overestimated fog density and longwave cooling. The turbulent exchange with the surface may decrease too much under Ri_{max}=1.0, which must be tested in more and longer experiments as well as in different domains before this can be concluded.

The current longwave emissivity of liquid water droplets in Harmonie a_{cl} is based on idealized atmo-

spheric conditions in 1978 and too high for our time and domain. Based on Cabauw measurements of five years of nighttime radiation fog events a reduction of a_{cl}=0.144 to a_{cl}=0.096 is proposed. The fog development turns out to be very sensitive to this reduction, strongly decreasing in spatial extent as well as radiative cooling and fog density. However, especially over sea, fog expansion is still overestimated. Combining a_{cl}=0.096 with a lowered inhomogeneity factor from 1.0 to 0.7 further reduces fog expansion, but this is physically not defendable and should therefore be avoided.

An important conclusion that can be drawn from the series of experiments in both Musc and Harmonie is the large sensitivity of fog development to the parameter CCN in ICE3. When CCN is reduced, droplet condensation processes are inhibited leading to a lower cloud water content. The positive feedback in which droplet condensation and longwave radiative cooling amplify each other is thereby reduced as well. From AROME-France experiments with LIMA it turns out that the inclusion of cloud droplet number evolution to the microphysical scheme brings cloud water concentrations back to observed values. In LIMA, cloud droplet concentrations decrease over time to values under 50 cm^{-3}. The cloud droplet concentration in ICE3 can be controlled by the parameter CCN, being constant over time. From LIMA and the experiments in this study it becomes clear that the currently prescribed CCN values in ICE3, which are 300 cm^{-3} for continental air masses and 100 cm^{-3} for maritime air masses, are too high for longer existing fog. When CCN is used as a tuning parameter, an optimal value will be between 10 cm^{-3} and 50 cm^{-3}. However, the general impact of such a change must be tested with more experiments and longer runs under different meteorological circumstances.

This research has shown some adaptations to Harmonie that have high potential to improve the model performance, but no conclusions can yet be drawn on the exact value of the specific parameters. Many combinations are possible, and due to the high complexity of Harmonie particular attention must be given to identify possible compensating errors. As experiment settings with a_{cl}=0.096 and CCN=25 or 50 cm^{-3} are currently expected to be a best estimate, these should be tested in a longer run to investigate their impact on other meteorological phenomena. For fine-tuning of the parametrizations, the analysis of many fog cases may contribute to a broader view, in the Netherlands but also in other domains that use Harmonie such as Ireland, Scandinavia and Spain. An already very positive result of this study is the revived discussion on problematic fog behavior by Harmonie experts of many HIRLAM

institutes. The results of this study showing the impact of CCN and emissivity, combined with the knowledge that KNMI and other HIRLAM institutes are working on further progress and evaluation, give confidence that fog simulation in future Harmonie versions can be improved.

13 Bibliography

1. American Meteorological Society. 2012. "Wavenumber - AMS Glossary." http://glossary.ametsoc.org/wiki/Wavenumber (September 26, 2019).
2. Bechtold, P. et al. 1995. "Modeling of Trade Wind Cumuli with a Low-Order Turbulence Model: Toward a Unified Description of Cu and Se Clouds in Meteorological Models." Journal of the Atmospheric Sciences 52(4): 455–63. http://journals.ametsoc.org/doi/abs/10.1175/1520-0469 (December 12, 2019).
3. van Beelen, Aldert J., and Aarnout J. van Delden. 2012. "Cleaner air brings better views, more sunshine and warmer summer days in the Netherlands." Weather 67.1: 21-25.
4. Bengtsson, Lisa et al. 2017. "The HARMONIE–AROME Model Configuration in the ALADIN–HIRLAM NWP System." Monthly Weather Review 145(5): 1919–35. http://journals.ametsoc.org/doi/10.1175/MWR-D-16-0417.1 (October 3, 2019).
5. Bergot, Thierry et al. 2007. "Intercomparison of Single-Column Numerical Models for the Prediction of Radiation Fog." Journal of Applied Meteorology and Climatology 46(4): 504–21. http://journals.ametsoc.org/doi/abs/10.1175/JAM2475.1 (December 19, 2019).
6. Bosveld, Fred C. 2019. Cabauw In-Situ Observational Program 2000-Now: Instruments, Calibrations and Set-Up. http://projects.knmi.nl/cabauw/insitu/observations/documentation/Cabauw_TR/Cabauw_TR.pdf (March 23, 2020).
7. Bougeault, Philippe. 1982. "Cloud-Ensemble Relations Based on the Gamma Probability Distribution for the Higher-Order Models of the Planetary Boundary Layer." Journal of the Atmospheric Sciences 39(12): 2691–2700. http://journals.ametsoc.org/doi/abs/10.1175/1520-0469 (December 12, 2019).
8. Bouteloup, Y., Y. Seity, and E. Bazile. 2011. "Description of the Sedimentation Scheme Used Operationally in All Météo-France NWP Models." Tellus A: Dynamic Meteorology and Oceanog-

raphy 63(2): 300–311.
https://www.tandfonline.com/doi/full/10.1111/j.1600-0870.2010.00484.x (October 17, 2019).

9. Cotton, William R., and Susan C. van den Heever. 2011. "Radiative Transfer in a Cloudy Atmosphere and Its Parameterization." International Geophysics 99: 143–75.
https://www.sciencedirect.com/science/article/pii/S0074614210099110 (October 21, 2019).
10. Donier, S et al. 2012. "Evaluation of the Impact of the Use of the ECOCLIMAP2 Database on AROME Operational Forecasts." Météo-France Technical Report.
https://www.umrcnrm.fr/surfex/IMG/pdf/test_eco2_arome. pdf (April 27, 2020).
11. Driesenaar, Tilly, and Patricia Pottier. 2014. pdfs.semanticscholar.org FROST-2014–Performance of Harmonie 1km during Sochi Olympics.
http://hirlam.org (April 27, 2020).
12. Duthon, Pierre, Michèle Colomb, and Frédéric Bernardin. 2019. "Light Transmission in Fog: The Influence of Wavelength on the Extinction Coefficient." Applied Sciences 9(14): 2843.
https://www.mdpi.com/2076-3417/9/14/2843 (October 15, 2019).
13. Duynkerke, Peter G. 1991. "Radiation Fog: A Comparison of Model Simulation with Detailed Observations." Monthly Weather Review 119(2): 324–41.
http://journals.ametsoc.org/doi/abs/10.1175/1520-0493 (October 1, 2019).
14. Duynkerke, Peter G. 1999. "Turbulence, Radiation and Fog in Dutch Stable Boundary Layers." Boundary-Layer Meteorology 90(3): 447–77.
http://link.springer.com/10.1023/A:1026441904734 (October 1, 2019).
15. Geleyn, J. F. et al. 2017. "Single Interval Longwave Radiation Scheme Based on the Net Exchanged Rate Decomposition with Bracketing." Quarterly Journal of the Royal Meteorological Society 143(704): 1313–35.
16. Gultepe, I, G.A. Isaac, and K.B. Strawbridge. 2001. "Variability of Cloud Microphysical and Optical Parameters Obtained from Aircraft and Satellite Remote Sensing Measurements during RACE." International Journal of Climatology 21(4): 507–25.
http://doi.wiley.com/10.1002/joc.582 (October 9, 2019).

17. Hess, M., P. Koepke, and I. Schult. 1998. "Optical Properties of Aerosols and Clouds: The Software Package OPAC." Bulletin of the American Meteorological Society 79(5): 831–44.
18. Khairoutdinov, Marat, Yefim Kogan, Marat Khairoutdinov, and Yefim Kogan. 2000. "A New Cloud Physics Parameterization in a Large-Eddy Simulation Model of Marine Stratocumulus." Monthly Weather Review 128(1): 229–43.
http://journals.ametsoc.org/doi/abs/10.1175/1520-0493 (December 12, 2019).
19. KNMI. "KNMI - Weerkaarten Archief Europa."
https://knmi.nl/nederland-nu/klimatologie/daggegevens/weerkaarten (May 2, 2020).
20. Kunkel, Bruce A. 1984. "Parameterization of Droplet Terminal Velocity and Extinction Coefficient in Fog Models." Journal of Climate and Applied Meteorology 23(1): 34–41.
http://journals.ametsoc.org/doi/abs/10.1175/1520-0450
21. Lascaux, Franck, Evelyne Richard, and Jean-Pierre Pinty. 2006. "Numerical Simulations of Three Different MAP IOPs and the Associated Microphysical Processes." Quarterly Journal of the Royal Meteorological Society 132(619): 1907–26.
http://doi.wiley.com/10.1256/qj.05.197 (October 17, 2019).
22. Lenderink, G., and A.A.M. Holtslag. 2004. "An Updated Length-Scale Formulation for Turbulent Mixing in Clear and Cloudy Boundary Layers." Quarterly Journal of the Royal Meteorological Society 130(604): 3405–27.
http://doi.wiley.com/10.1256/qj.03.117 (November 19, 2019).
23. Malardel, Sylvie, and Didier Ricard. 2015. "An Alternative Cell-Averaged Departure Point Reconstruction for Pointwise Semi-Lagrangian Transport Schemes." Quarterly Journal of the Royal Meteorological Society 141(691): 2114–26.
http://doi.wiley.com/10.1002/qj.2509 (November 19, 2019).
24. Martin, G. M. et al. 1994. "The Measurement and Parameterization of Effective Radius of Droplets in Warm Stratocumulus Clouds." Journal of the Atmospheric Sciences 51(13): 1823–42.
http://journals.ametsoc.org/doi/abs/10.1175/1520-0469
25. Mašek, J. et al. 2016. "Single Interval Shortwave Radiation Scheme with Parameterized Op-

tical Saturation and Spectral Overlaps." Quarterly Journal of the Royal Meteorological Society 142(694): 304–26.

26. Masson, Valéry et al. 2003. "A Global Database of Land Surface Parameters at 1-Km Resolution in Meteorological and Climate Models." Journal of Climate 16(9): 1261–82. http://journals.ametsoc.org/doi/abs/10.1175/1520-0442-16.9.1261 (April 27, 2020).
27. Mazoyer, Marie et al. 2019. "Experimental Study of the Aerosol Impact on Fog Microphysics." Atmospheric Chemistry and Physics 19(7): 4323–44. https://www.atmos-chem-phys.net/19/4323/2019/ (April 21, 2020).
28. Meseguer, José, Isabel Pérez-Grande, and Angel Sanz-Andrés. 2012. "Thermal Radiation Heat Transfer." In Spacecraft Thermal Control, , 73–86. https://content.taylorfrancis.com/books/download?dac=C2012-0-15956-5 isbn=9780429190599format=googlePreviewPdf (October 15, 2019).
29. Mlawer, Eli J. et al. 1997. "Radiative Transfer for Inhomogeneous Atmospheres: RRTM, a Validated Correlated-k Model for the Longwave." Journal of Geophysical Research: Atmospheres 102(D14): 16663–82. http://doi.wiley.com/10.1029/97JD00237 (October 17, 2019).
30. Müller, Malte et al. 2017. "AROME-MetCoOp: A Nordic Convective-Scale Operational Weather Prediction Model." Weather and Forecasting 32(2): 609–27. http://journals.ametsoc.org/doi/10.1175/WAF-D-16-0099.1 (December 12, 2019).
31. Niemelä, Sami, Petri Räisänen, and Hannu Savijärvi. 2001. "Comparison of Surface Radiative Flux Parameterizations: Part I: Longwave Radiation." Atmospheric Research 58(1): 1–18. https://www.sciencedirect.com/science/article/pii/S0169809501000849 (October 1, 2019).
32. OFCM. 2005. Federal Meteorological Handbook Number 1: Surface Weather Observations and Reports. Office of the Federal Coordinator for Meteorology. http://www.ofcm.gov/fmh-1/pdf/H-CH8.pdf (September 23, 2019).
33. Van Oldenborgh, G. J., P. Yiou, and R. Vautard. 2010. "On the Roles of Circulation and Aerosols in the Decline of Mist and Dense Fog in Europe over the Last 30 Years." Atmospheric Chemistry

and Physics 10(10): 4597–4609.
https://www.knmi.nl/kennis-en-datacentrum/publicatie/on-the-roles-of-circulation-and-aerosols-in-the-decline-of-mist-and-dense-fog-in-europe-over-the-last-30-years (March 17, 2020).

34. Park, Shinfield. 2012. "IFS Documentation - Part IV: Physical Processes." ECMF IFS documentation (June): 189.
https://www.ecmwf.int/node/16648.
35. Petersen, Claus., Niels Woetmann. Nielsen, and Danmarks meteorologiske institut. 2000. Diagnosis of Visibility in DMI-HIRLAM. DMI.
36. de Rooy, W. 2014. "The Fog above Sea Problem in Harmonie: Part 1 Analysis." hirlam.org.
http://www.hirlam.org/index.php/hirlam-documentation/doc_view/1490-aladin-hirlam-newsletter-no-2-april-2014page=10 (October 3, 2019).
37. Shah, Shahnawaz, Samreen Mughal, and Shahzad Memon. 2015. "Theoretical and Empirical Based Extinction Coefficients for Fog Attenuation in Terms of Visibility at 850 Nm." In 2015 International Conference on Emerging Technologies (ICET), IEEE, 1–4.
http://ieeexplore.ieee.org/document/7389190/ (October 15, 2019).
38. Simmons, A. J., and D. M. Burridge. 1981. "An Energy and Angular-Momentum Conserving Vertical Finite-Difference Scheme and Hybrid Vertical Coordinates." Monthly Weather Review 109(4): 758–66.
http://journals.ametsoc.org/doi/abs/10.1175/1520-0493
39. Steeneveld, G. J., R. J. Ronda, and A. A. M. Holtslag. 2015. "The Challenge of Forecasting the Onset and Development of Radiation Fog Using Mesoscale Atmospheric Models." Boundary-Layer Meteorology 154(2): 265–89.
http://link.springer.com/10.1007/s10546-014-9973-8 (October 2, 2019).
40. Stephens, Graeme L. 1983. "The Influence of Radiative Transfer on the Mass and Heat Budgets of Ice Crystals Failing in the Atmosphere." Journal of the Atmospheric Sciences 40(7): 1729–39.
http://journals.ametsoc.org/doi/abs/10.1175/1520-0469
41. Sun, Zhian. 2001. "Reply to Comments by Greg M. McFarquhar on 'Parametrization of Effective

Sizes of Cirrus-Cloud Particles and Its Verification against Observations'. (October B, 1999,125, 3037–3055)." Quarterly Journal of the Royal Meteorological Society 127(571): 267–71. http://doi.wiley.com/10.1002/qj.49712757116 (December 11, 2019).

42. Sun, Zhian, and Lawrie Rikus. 2007. "Parametrization of Effective Sizes of Cirrus-Cloud Particles and Its Verification against Observations." Quarterly Journal of the Royal Meteorological Society 125(560): 3037–55. http://doi.wiley.com/10.1002/qj.49712556012 (December 11, 2019).
43. Tegen, Ina et al. 1997. "Contribution of Different Aerosol Species to the Global Aerosol Extinction Optical Thickness: Estimates from Model Results." Journal of Geophysical Research: Atmospheres 102(D20): 23895–915. http://doi.wiley.com/10.1029/97JD01864 (December 11, 2019).
44. Tiedtke, M. 1996. "An Extension of Cloud-Radiation Parameterization in the ECMWF Model: The Representation of Subgrid-Scale Variations of Optical Depth." Monthly Weather Review 124(4): 745–50.
45. Tijm, Sander. 2019. Predicting Low Clouds, Fog and Visbility: Experiences and Ideas for Future Strategy. https://www.umr-cnrm.fr/aladin/IMG/pdf/bent-2.pdf.
46. Tijm, Sander and Dienenveen, Jos. 2019. Model Performance 11-18 April.
47. Toll, V. et al. 2016. "Impacts of the Direct Radiative Effect of Aerosols in Numerical Weather Prediction over Europe Using the ALADIN-HIRLAM NWP System." Atmospheric Research 172–173: 163–73. https://www.sciencedirect.com/science/article/pii/S0169809516000144 (December 11, 2019).
48. Vautard, R, P Yiou, and G J Van Oldenborgh. 2009. "The Decline of Fog , Mist and Haze in Europe during the Last 30 Years: A Warming Amplifier?" Assembly 11: 8473. https://www.knmi.nl/kennis-en-datacentrum/publicatie/the-decline-of-fog-mist-and-haze-in-europe-during-the-last-30-years-a-warming-amplifier (March 17, 2020).
49. Wærsted, Eivind G. et al. 2017. "Radiation in Fog: Quantification of the Impact on Fog Liquid

Water Based on Ground-Based Remote Sensing." Atmospheric Chemistry and Physics.

50. World Meteorological Organization. 1983. "Guide to Meteorological Instruments and Methods of Observation." (October 15, 2019).

51. Yamamoto, Giichi, Masayuki Tanaka, and Shoji Asano. 1970. "Radiative Transfer in Water Clouds in the Infrared Region." Journal of the Atmospheric Sciences 27(2): 282–92. http://journals.ametsoc.org/doi/abs/10.1175/1520-0469 (December 5, 2019).